

Sedimentary response to the contrasting provenance and oceanographic conditions on the continental shelf of India

N. Kadam^{1,2}, F. Badesab^{1*}, V. Gaikwad^{1,2}, M. Kotha², L.L. Fernandes¹, M. Venkateshwarlu³

¹CSIR- National Institute of Oceanography, Dona Paula, Goa, 403004, India

²School of Earth Ocean and Atmospheric Sciences, Goa University, 403206, Goa, India

³CSIR–National Geophysical Research Institute, Uppal Road, Hyderabad 500007, India

*Corresponding Author: Dr. Firoz Badesab (firoz@nio.org)

Abstract

The present study sets out to elucidate how magnetic minerals derived from wide array of source regions respond to shelfal sedimentary processes in a complex shelf system. The sediment magnetism is primarily governed by complex magnetic mineral assemblages (magnetite, titanomagnetite, titanohematite) of detrital origin, with variable concentration and grain sizes. A clear trend of decline in magnetite content coupled with fining of magnetic crystal size in the studied sediment cores can be attributed to prominent change in magnetic mineral contribution from mafic to felsic dominated sediment province. The sediments exhibiting elevated magnetite content manifested by fine and coarse-grained magnetic particles and mere variations in terms of magnetic mineralogy can be linked with the increased magnetic contribution from the Deccan basalt (DcB) in the shelf sediments off Narmada, Tapti, Mahi, and Sabarmati (NTMS) river system, Arabian Sea. A distinct shift in magnetite content accompanied by abrupt fluctuations in clastic grain size in core off Ganga-Brahmaputra (G-B) shelf, Bay of Bengal indicate the major change in detrital sedimentation. A major change in the magnetic mineralogy diagnostic proxy (S-ratio) manifested by increased supply of titanomagnetite particles marks the onset of mafic sourced material in the sediments off Pennar – Swarnamukhi (P-S) shelf, Bay of Bengal. Successive mixing of mafic source derived material with felsic rich sediments driven by alongshore littoral drift system is clearly recorded in the bivariate plot of magnetic parameters of the shelf sediments off P-S. Magnetogranulometry data revealed that magnetic crystal size is independent of physical grain size above $>40\ \mu\text{m}$ in NTMS and G-B, and $>20\ \mu\text{m}$ in P-S samples. Decoupling between these parameters is mainly due to polycrystalline nature, where fine-grained magnetic particles occurred as inclusions within silt and sand fractions. We demonstrate that integrated approach combining rockmagnetic, mineralogical and sedimentological methods can be effectively used to assess the influence of the contrasting provenance and oceanographic conditions on the dispersal and deposition of magnetic particle in the shelf systems.

Key Words: Continental Shelf, Magnetic Minerals, Rock Magnetism, Provenance, Hydrodynamics, Magnetogranulometry

Highlights:

- Unravels the control of contrasting lithologies and shelfal hydrodynamics on the dispersal and deposition of magnetic particles in the shelf system.
- Sediment magnetism is mainly carried by detrital magnetic particles occurring as discrete as well as fine-grained inclusions in silicate grains.
- Magnetic signatures of shift in sediment provenance and grain size linked with prominent change in magnetic contribution from mafic to felsic dominated sediment province.
- Magnetic inclusion in silicate minerals precludes signature of changing sediment provenance and fractionation processes. Magnetogranulometry approach for efficient tracking of sedimentary processes in the shelf system.

1. Introduction

Continental shelf sediments provide a unique archive of the sedimentary processes and preserves a record of changes in detrital inputs and dispersal system through geologic time (Chiocci and Chivas, 2014; Gao and Collins, 2014; Caricchi et al., 2018). Contrasting lithologies, varied drainage basin morphometry, climate-controlled weathering and erosional processes in the hinterlands and fluvial and marine hydrodynamics at the sink region control the production, storage, sorting, dispersal and deposition of sediments within the basin, nearshore, and shelf region (Hatfield, 2014; Kissel et al., 2016; Wang et al., 2017). Magnetic minerals are ubiquitous and potential recorders of geological and hydrodynamic processes in the shelf system (Thompson and Oldfield, 1986; Roberts, 2015). Provenance controls the magnetic mineralogy, while the concentration and grain size characteristics is governed by the hydraulic regime and the depositional environment. Composition (type of magnetic minerals), texture (shape, grain size), physical properties (grain density, packing), amount of detrital input, shelf morphology and interplay between river runoff, tidal currents and waves control the mixing, fractionation, enrichment and dispersal of magnetic particles (Thompson and Oldfield, 1986; Liu et al., 2012; Hatfield, 2014). Hence, magnetic minerals have been successfully used as excellent markers to investigate the sedimentary processes in shelf systems.

Rock magnetism is a well-established method and mainly focusses on utilizing mineral and grain-size specific magnetic properties of sediments (Evans and Heller, 2003; Liu et al., 2012). This method has been successfully applied to marine shelf systems for example, to elucidate the sediment provenance linked with shifts in Asian summer monsoon in the inner shelf sediments of the East China Sea (Wang et al., 2020), evaluate the control of provenance, weathering and erosional processes on the composition of sediments along the South American continental shelf (Nagai et al., 2014), inner shelf of northern Gulf of Mexico (Pepper and Stone, 2004), South China Sea (He et al., 2020) and Southeast Brazil (Cruz et al., 2018), and unravel the influence of diagenesis on the magnetic properties of SE Mediterranean Continental Shelf sediments (Amiel et al., 2020), East China Sea (Ge et al., 2015) and off Gambia, NW Africa (Just et al., 2012). In Indian context, several researchers successfully utilized rock magnetic method on the shelf sediments to develop the magnetic mineral inventory of the surface sediments (Sebastian et al., 2019a), unravel the control of provenance changes and monsoon-driven weathering and erosional processes on the sediment magnetic records (Sangode et al., 2001, Rao et al., 2010; Kulkarni et al., 2014; Dash et al., 2022), assessment of heavy metal concentrations (Alagarsamy, 2009), impact of the Indian Summer Monsoon variability on the source area weathering (Sebastian et al., 2019b). However, a dedicated

rock magnetic study aimed at deepening fundamental understanding on the control of geological and hydrodynamic processes on the magnetic properties of shelf sediments was still lacking.

Continental shelf sediments along the eastern (ECMI) and western (WCMI) margin of India are derived from different sources and preserve a specific magnetic signature. Geological setting dominated by igneous (Deccan Basalts-DcB), metamorphic (Archean-Proterozoic Gneissic Complexes-APGC), and Sedimentary rocks (Quaternary sediments) in the catchment areas and well-developed peninsular and Himalayan Rivers draining through these terrains assure high supply of detrital magnetic minerals to the ECMI and WCMI. The sediment dynamics (transport, dispersal, deposition) along each littoral and shelf system of ECMI and WCMI is distinct, region specific and largely controlled by the combined influence of differential continental inputs and varying sedimentation processes. A better understanding of magnetic mineral assemblages and concentration processes in such systems can help not only to detect the shifts in the sediment provenance, but also to reveal details of the underlying hydro- and sediment dynamics. Three sediment (gravity) cores retrieved off western (SSK-40/GC-07; Arabian Sea), and eastern (SSK-35/GC-14; SSK-50/GC-14; Bay of Bengal) continental shelf (Fig. 1) of India preserve an exemplary record and are ideal for elucidating the shelfal sedimentary processes driven by contrasting lithologies and hydro- and sediment dynamics. A comprehensive approach involving rock magnetism, granulometry, and mineralogical methods is employed on the shelf (ECMI, WCMI) sediments for studying the source-to-sink related processes. The present study sets out to address two key research questions:

- (a) How does magnetic mineral compositional variability exerted by contrasting provenance, differential fluxes and changing hydrodynamic regime constrain the dispersal and deposition of magnetic particles in the shelf system?
- (b) How does different size magnetic particles derived from wide array of source regions respond to shelfal sedimentary (mixing, fractionation, settling, dispersal) processes?

2. Study area, catchment geology and river systems

The Narmada River basin is a pericratonic rift basin in which the Narmada River flows along the Son-Narmada lineament, which segments the Indian peninsula into two diverse geological domains (Verma and Banerjee, 1992). The Narmada, Tapi, Mahi and Sabarmati (NTMS) are the major river systems which delivers large sediment load to the WCMI. Indian south-west (SW) monsoon control the weathering and erosional processes in the catchment areas of the NTMS system. The NTMS river systems drain through Deccan Trap basalts, Precambrian Peninsular gneissic complex and quaternary alluvium/sediments followed by the Proterozoic Vindhyan and

Gondwana Supergroup (sandstone, limestone, mudstone, shale, quartzite, phyllite, dolomite, conglomerates), Aravalli Supergroup (phyllite, quartzite, metavolcanic and conglomeratic) and banded gneissic complex rocks and deliver the sediments to the WCMI (Gupta and Chakrapani, 2005; Ramakrishnan and Vaidyanathan, 2010; Fig. 1).

The sediments of ECMI are mainly derived from the Himalayan and Peninsular Indian sources. The Ganga and Brahmaputra (G-B) River system feeds the largest Bengal delta and deep-sea fan in the world (Coleman, 1969, Milliman and Meade, 1983, Singh et al., 2007, Rahman et al., 2018; Fig. 1). Most of the sediments from G-B river system are derived from the tectonically active Himalayan orogen. The catchment rocks of Ganga river comprised of sedimentary sequences of clastic and carbonate rocks belonging Paleozoic to Eocene age, gneisses, migmatites and highly metamorphosed (amphibolite facies) sedimentary rocks, Proterozoic ortho-gneisses, metasedimentary, Paleozoic and Cenozoic rocks (Garzanti, 1999; Decelles et al., 2001; Singh et al., 2007). The Brahmaputra River drains through Trans Himalayan batholiths, ophiolites, turbidites granitoid gneisses and Cenozoic turbidites, ophiolite melanges (Garzanti et al., 2019). Contribution from Indian peninsular terrains is minor compared to Himalayan orogen (Goodbred, 2003, Singh et al., 2007).

The Penner and Swarnamukhi (P-S) are the major river systems feeding the southeastern region between Krishna and Cauvery basins of the Indian Peninsula. Most of the sediments in the P-S Rivers are derived from Dharwar System Rocks lithology comprised of peninsular gneisses (Tonalite-Trondjemite-granodiorite suite), shale, limestone and quartzite sequences of Proterozoic Cuddappah Supergroup, younger granites, feldspathic sandstone, dolomitic limestone, stromatolitic limestone (with mafic sills, dykes), granitic-gneissic terrains, and Quaternary sediments (Anand et al., 2003; Ramakrishnan and Vaidyanathan, 2010; Patel et al., 2020). Detailed information on the river systems including river length, drainage area and sediment load are presented in Table 1.

3. Materials and methods

3.1. Sub-sampling of sediment cores

Three sediment (gravity) cores retrieved off the continental shelf NTMS (SSK-40/GC-07), G-B (SSK-35/GC-14), and P-S (SSK-50/GC-14) rivers during the oceanographic cruises SSK-35, SSK-40, and SSK-50 onboard research vessel R/V Sindhu Sankalp. More details regarding the location, water depth, recovered length of sediments cores are provided in Table 2. The sediment cores were initially cut into one metre each and stored at the cold storage facility onboard. After the completion of the cruises, the sediment cores were transported and further stored at ~5–6 °C at the cold

repository of CSIR-National Institute of Oceanography (CSIR-NIO), Goa, India. At CSIR-NIO, the entire sediment cores were sub-sampled at intervals of 1-2 cm following standard Ohio EPA Sediment Sampling Guide (Taft and Jones, 2001). For rock magnetic analyses, the sub-samples were dried, weighed and packed into 25 mm cylindrical non-magnetic plastic bottles.

3.2. Rock magnetic measurements

Low and high field magnetic susceptibility (χ_{lf}) measurements were carried out using the Bartington Instrument MS2B dual frequency susceptibility meter. The susceptibility was measured at two different frequencies $\chi_{lf} = 0.47$ kHz and $\chi_{hf} = 4.7$ kHz. Anhyseretic remanent magnetization (ARM) was imparted by applying a decaying 100 mT alternating magnetic field (AC) with a steady direct current (DC) bias field of 50 μ T on a Molspin alternating field (AF) demagnetizer with a pARM attachment. An isothermal remanent magnetization (IRM) was applied in an inducing fields in the forward direction and was demagnetized by DC backfields at - 20 mT, - 30 mT, - 100 mT and - 300 mT using a MMPM10 pulse magnetizer. The respective remanences (ARM, IRM) were measured using AGICO JR-6A automatic dual speed spinner magnetometer (AGICO, Czech Republic) (Sensitivity- 2.4×10^{-6} A/m). We have considered the mass-normalized IRM acquired at a peak field of +1T as the saturation isothermal remanent magnetization (SIRM) in the sediment samples off NTMS as the bulk magnetic mineralogy is mainly dominated by ferrimagnetic (titanomagnetite) particles. In G-B and P-S samples, a peak field of +2.5 T was considered as SIRM as the bulk magnetic mineralogy is dominated by ferri-(titanomagnetite) and antiferromagnetic (titano hematite) particles. Magnetic susceptibility and remanence measurements were carried out at the paleomagnetic laboratory of CSIR-NIO, Goa, India. The hysteresis loops and thermomagnetic curves of representative samples were generated on the advanced variable field translation balance (AVFTB) (max. field - 1T, temperature range: 0 - 700 °C) at the paleomagnetic laboratory of CSIR-National Geophysical Research Institute (NGRI), Hyderabad.

3.3. Rock magnetic parameter estimation

The data of magnetic susceptibility and acquired remanence was first converted into the mass normalized values. Magnetic mineralogy diagnostic parameter S-ratio ($S_{0.3T}$) was estimated using the ratio $S_{0.3T} = [(-IRM_{-300mT}/SIRM)+1]/2$ (Bloemendal et al., 1992). The magnetite content was estimated by dividing the magnetic susceptibility values of analysed sediment samples by the standard magnetic susceptibility value of pure multidomain (MD) magnetite (660×10^{-6} m³/kg) (Maher, 1988). The coercivity of remanence (H_{cr}) values were calculated from the backfield

remanence data. Necessary parameters were extracted from the magnetic hysteresis data for identification of magnetic domain state.

3.4. Magnetogranulometry on sieved fractions

Eighteen samples representing different sediment depth intervals of all three cores were selected for magnetogranulometric analyses. Bulk sediment samples of 30 g were dried, weighed, and suspended in a 1000 ml distilled water. Prior to wet-sieving, about 200 mg of a sediment dispersing agent ($\text{Na}_4\text{P}_2\text{O}_7 \times 10 \text{ H}_2\text{O}$) was added to the bulk sediment suspension and treated with ultrasonics for better dispersion. The sediment suspensions were wet-sieved for 20 mins with an automated sieve shaker (Fritsch Analysette 3, optimum amplitude) creating three particle size fraction 20-40 μm , 40-63 μm , and >63 μm . The fractions of size <4 μm and 4-20 μm were created by manually sieving of the <20 μm (left over sediment slurry from the sieve shaker). Each separated fractions were dried, weighed and mounted centrally into the 25 mm non-magnetic cylindrical plastic bottles and were further subjected to the magnetic measurements.

3.5. Scanning electron microscopy-energy dispersive spectrum (SEM-EDS), optical microscopy and X-ray diffraction analyses (XRD)

Magnetic particles were extracted from the bulk sediment samples following the procedure of Peterson et al. (1986). The magnetic particles were then mounted on the copper stubs. High-resolution scanning electron microscope (SEM) images were acquired using JOEL JSM 5800 LV in a secondary electron (SE) imaging mode at 5 and 20 keV energy levels. The composition of magnetic particles was determined using an energy dispersive spectrum (EDS) probe attached to the microscope. Optical microscopy was carried out on the separated >63 μm fractions using Nikon SMZ18 stereoscopic microscope. Magnetic minerals were identified using a Rigaku X-Ray Diffractometer (XRD) (Ultima IV). Magnetic mineral extract of NTMS and bulk (powdered) sediments of G-B and P-S samples were mounted on a slide containing a depression prior to XRD analyses. The samples were run from 10° to 70° 2θ at $1^\circ/\text{min}$ scan speed using Cu $K\alpha$ radiation ($\lambda = 1.5414 \text{ \AA}$). Mineral phases were identified using software 'Match-Phase analysis using powder diffraction' (<http://www.crystalimpact.com/match/>).

3.6. Granulometric analyses

The sediment grain size distributions were measured using a Beckman Coulter LS 13 320 laser diffraction particle size analyzer (range: 0.0017 to 2000 μm) at the National Centre for Polar and Oceanic Research (NCPOR), Goa, India. About two hundred and ten sediment samples representing three sediment cores were first desalinated and later treated with dilute hydrochloric

acid (1N) and 10% solution of hydrogen peroxide for removal of organic carbon and carbonate content. The treated samples were washed multiple times. The dispersing agent (sodium hexametaphosphate) was added and the sediment suspensions were treated with ultrasonics prior to the measurements.

4. Results

4.1. Down-core changes in the rock magnetic properties

Magnetic susceptibility (χ_{lf}) and saturation isothermal remanent magnetization (SIRM) are sensitive to the concentration of magnetic minerals, while ARM/SIRM and S-ratio are diagnostic proxy for magnetic grain size and mineralogy respectively (Thompson, 2012). The rock magnetic properties of sediment cores from the shelf off NTMS (Fig. 2a-2f), off G-B (Fig. 3a-3e), and off P-S (Fig. 4a-4e) rivers are described below. In the sediment core off NTMS (SSK-40/GC-07), we defined three (Z-I, Z-II, Z-III) distinct sediment magnetic zones based on the changes in the magnetic susceptibility (χ_{lf}) (Fig. 2). In general, the χ_{lf} values vary between 34.78 to 47.68 x 10⁻⁶ m³ kg⁻¹. The uppermost sediment magnetic zone (Z-I: 0.05 to 23 cmbsf) is marked by higher values of χ_{lf} and SIRM relative to Z-III (Fig. 2a, 2c), but exhibit minor down-core reduction in χ_{lf} (min = 39.36 x 10⁻⁶ m³ kg⁻¹, max = 42.28 x 10⁻⁶ m³ kg⁻¹). The Z-II (24 to 125 cmbsf) exhibit relatively elevated and near consistent values of χ_{lf} and SIRM indicating the dominant presence of ferrimagnetic particles in higher concentration (min = 39.11 x 10⁻⁶ m³ kg⁻¹, max = 42.28 x 10⁻⁶ m³ kg⁻¹, Avg = 47.68 x 10⁻⁶ m³ kg⁻¹; Fig. 2a, 2c). A systematic down-core reduction in concentration of magnetic particles is clearly visible in Z-III (126 – 279 cmbsf) as seen through decline in χ_{lf} and SIRM (Fig. 2a, 2c). The magnetic grain size proxy (ARM/SIRM) profile showed two major and consistent patterns (Fig. 2e). Overall, ARM/SIRM values ranges between 0.02 to 0.03 (Fig. 2e). The Z-I and Z-II showed a gradual decrease in ARM/SIRM values indicating the coarsening of magnetic particles, while the Z-III clearly exhibit opposite trend of fining of magnetic particles (Fig. 2e). A good covariation between χ_{lf} and magnetic grain size proxy (ARM/SIRM) is noticed ($R^2 = 0.43$, $R = -0.65$, $p < 0.05$; Fig. 2c, 2e). The samples possessing higher χ_{lf} were linked with the coarser magnetic particles and vice versa. Magnetic mineralogy diagnostic proxy (S-ratio) showed more uniformity and the values ranges between 0.95 to 0.99 suggesting the dominance of ferrimagnetic minerals (Fig. 2d). A shift in S-ratio is seen at 180 cmbsf.

The rock magnetic record of sediment core off G-B (SSK-35/GC-14) exhibit significantly different magnetic characteristics compared to other cores (NTMS, P-S) interms of magnetic mineral concentration, grain size and mineralogy (Fig. 3a, 3b, 3c). We noticed a marked change in χ_{lf} and

SIRM at 110 cmbsf (Fig. 3a, 3c). Overall, the magnetite concentration in this core varies between 0.37 to 0.57 % (Table 2) and exhibit significantly lower χ_{lf} and SIRM values compared to sediment cores off NTMS and P-S rivers (Fig. 3 and Table 2). Large variation in ARM/SIRM (0.02 to 0.06) record suggest the presence of both fine and coarse-grained magnetic particles in this core (Fig. 3e). The lowermost sediment interval (221 to 252 cmbsf) showed low ARM/SIRM values indicative of the presence of coarser magnetic particles (Fig. 3e). S-ratio showed large fluctuation and the values range from 0.83 to 0.99 suggesting the presence of mixed (ferri-and antiferro) type magnetic mineralogy (Fig. 3d).

The rock magnetic record of sediment core off P-S (SSK-50/GC-14) showed cyclic variability interms of magnetic mineral concentration (min = $0.95 \times 10^{-6} \text{ m}^3 \text{ kg}^{-1}$, max = $10.38 \times 10^{-6} \text{ m}^3 \text{ kg}^{-1}$; Fig. 4a, 4b, 4c) and can be futher defined into four distinct sediment magnetic zones (Z-I, Z-II, Z-III, Z-IV). Zones Z-I and Z-III exhibited higher χ_{lf} and SIRM values compared to Z-II and Z-IV reflecting the dominance of ferrimagnetic particles in these zones. Two distinct trends exhibiting large variation in magnetic mineralogy is evident in S-ratio profile (0.72 to 0.99; Fig. 4d). The sediment magnetic zones (Z-I to Z-III) showed higher and consistent S-ratio values suggesting the predominance of ferrimagnetic particles. Contrastingly, Z-IV showed remarkably lower and relatively stable S-ratio (Fig. 4d) values indicating the dominance of antiferromagnetic (high coercive) particles in this zone. The ARM/SIRM record (Fig. 4e) revealed that Z-II to Z-IV are dominated by coarse-grained magnetic particles as seen through lower ARM/SIRM values in these zones. Comparatively, Z-I is dominated by the finer magnetic particles as seen through elevated ARM/SIRM values (Fig. 4e).

4.2 Magnetic mineralogy and grain size diagnostic proxies: Thermomagnetic curves and Day-Dunlop plot

Temperature-dependent magnetization curves provided confirmation on the magnetic mineralogy based on their individual curie temperatures (Liu et al., 2012). The thermomagnetic curves of sediment core off NTMS (SSK-40/GC-07) display similar pattern of heating and cooling cycles (Fig. 5a, 5b). A gradual decline in susceptibility values above 500 °C followed by sharp reduction between 533 °C and 550 °C suggests that the bulk magnetic mineralogy is domination by magnetite (Ti-rich) (Dunlop and Ozdemir, 1997; Fig. 5a, b). A minor enhancement in the magnetization between 533 °C and 550 °C could be either attributed to the conversion of paramagnetic minerals (for example, pyrite and iron-bearing silicates, iron-rich carbonates, siderite, and iron-rich smectites) into magnetite during heating process (Fig. 5b; Hirt and Gehring, 1991; Passier et al., 2001) or due to

the presence of titanomagnetite which display a wide range of Ti-contents (Dunlop and Ozdemir, 1997; Lattard et al., 2006).

In sediment cores off G-B (SSK-35/GC-14) and P-S (SSK-50/GC-14), a sharp decline in χ between 552 °C and 633 °C in most of the samples imply that the bulk magnetic mineralogy is mainly governed by magnetite (Fig. 5c, 5e; Dunlop and Ozdemir, 1997). A prominent rise in χ between 300 °C and 500 °C in few samples can be attributed to the conversion of paramagnetic minerals into magnetite during heating cycle (Fig. 5c, 5e; Hirt and Gehring, 1991; Hirt et al., 1993; Pan et al., 2000; Passier et al., 2001; Cui et al., 2017; Philips, 2018). Day-Dunlop plot of representative samples from sediment cores off G-B (SSK-35/GC-14) and P-S (SSK-50/GC-14) showed large variability in magnetic grain sizes and majority of the samples fall on the SP-SD and SD-MD mixing lines (Fig. 6). Contrastingly, the NTMS samples showed less fluctuation and mainly lie within the PSD range (Fig. 6).

4.3 Mineralogical analyses of magnetic particles

4.3.1. Scanning Electron Microscopy (SEM) and Energy Dispersive Spectra (EDS) Analysis on Magnetic Separates

A comprehensive SEM-EDS analyses on the magnetic particles complement our rock magnetic observations and further confirmed that titanomagnetite, titanohematite and magnetite are the major magnetic minerals in the studied sediment cores (Figs. 7, S10). Detrital magnetite and titanomagnetites (Fe-Ti) of diverse morphology (size, shape) constitute the dominant magnetic mineralogy of all sediment cores (Figs. 7, S1, S2, S3, S10). Magnetically enhanced shelf sediments off NTMS (SSK-40/GC-07) showed the abundant presence of detrital Fe-Ti grains with variable titanium content, which is clearly evident from Ti-peaks revealing the stoichiometric differences within the magnetic phases (Fig. S10). The sharp edges, clear/smooth faces and idiomorphic texture of crystals reveal detrital nature of magnetic minerals (Figs. 7a, 7b, 7d, 7e, 7f, 7g, S1, S2, S3). Surface etching and shrinkage cracks indicative of low-temperature maghemitization were observed on few Fe-Ti grains (Figs. 7h, S1i, S2c, S2i; Nowaczyk, 2011).

The magnetic mineralogy in shelf sediments off G-B (SSK-35/GC-14) mainly comprised of detrital magnetite and Fe-Ti particles (Figs. 8, S4, S5, S6, S11). Large variation interms of composition and morphology of magnetic particles are noticed. For example, surficial shrinkage cracks, very fine fractures and peeled layers indicative of maghemitization of Fe-Ti particles are observed (Figs. 8c, 8f, 8h, S4h, S5a, S5d, S5h, S5f, S6a, S6f, S6c). Lamellar texture of magnetic particles along with less prominent peaks of iron and oxygen suggest the presence of

antiferromagnetic (titanohematite) mineral in this zone (Z- II, Figs. 8i, S6d; Nowaczyk, 2011). It is interesting to note that pure octahedral to highly irregular shape of magnetite with compositional variability (i.e., magnetite to titanomagnetite) are noticed implying heterogeneity in the source rock composition (Figs. 8d, 8g).

The magnetic particles in the shelf sediments off P-S (SSK-50/GC-14) comprised of detrital Fe-Ti particles (Figs. 9, S7, S8, S9, S12). Diagenetically formed pyrite occur as framboid as well as fine-grained individual crystals in the bottommost sediment magnetic zone (Z-IV) marked by lower χ_{lf} (Fig. 4a). Signatures of low-temperature maghemitization of detrital Fe-Ti particles including distinct shrinkage cracks on the surface are noticed (Figs. 9b, 9d, S7c, S7g, S8c). Etching of surface, irregular cracks, pitted and dissolved corners of magnetic particles are observed (Figs. 9f, 9i, S8h, S9g, S9h, S9i). A skeleton lamellar structure typical characteristic feature of titanohematite formed due to diagenetic dissolution is seen in the sediment magnetic zone Z-IV, which is also marked by lowest S-ratio and χ_{lf} (Figs. 9i, S9i).

4.3.2. Identification of magnetic minerals using X-ray diffraction (XRD) analysis

XRD curves of magnetic minerals representing different sediment cores are displayed in Fig. 10. XRD data revealed that magnetite (M), titanomagnetite (TM) and titanohematite (TH) are the predominant ferri-and antiferro (titanohematite) magnetic minerals and largely governed the bulk sediment magnetism. In addition, quartz (Qz) and calcite (Ct) are the non-magnetic minerals identified in the analyzed sediment core samples.

4.4. Relationship between rock magnetic parameters and sediment grain size

Bivariate data plots revealed large variations in the magnetic mineral concentration, mineralogy and grain size between shelf sediments (Fig. S13). Three distinct grouping between the sediments exhibiting similar magnetic and grain size characteristics is clearly evident (Fig. S13). A good relationship between χ_{lf} and SIRM is observed in cores off NTMS ($R^2 = 0.78$, $R = 0.87$, $p < 0.05$) and P-S ($R^2 = 0.96$, $R = 0.98$, $p < 0.05$) (Fig. S13a). A strong covariation between χ_{lf} and ARM/SIRM is clearly visible especially in the NTMS ($R^2 = 0.43$, $R = -0.65$, $p < 0.05$) and P-S ($R^2 = 0.17$, $R = 0.42$, $p < 0.05$) samples (Fig. S13b). Higher χ_{lf} values were found to be associated with coarse-grained magnetic particles and vice-versa. A trend of systematic covariation between concentration-dependent (χ_{lf}) and mineralogy (S-ratio) is observed (Fig. S13c). The NTMS samples display relatively higher values and narrow range in χ_{lf} and S-ratio values suggesting the dominance of ferrimagnetic particles sourced from DcB (Fig. S13c). Contrastingly, P-S samples showed wide

range in χ_{lf} and S-ratio values implying the presence of mixed (soft and hard coercive) type magnetic mineral assemblage (Fig. S13c).

Good covariation between χ_{lf} and mean grain size is observed only in NTMS samples ($R^2 = 0.53$, $R = 0.73$, $p < 0.05$; Fig. S13d). Similarly, good correlation between ARM/SIRM and sediment mean grain size is seen in NTMS ($R^2 = 0.74$, $R = -0.86$, $p < 0.05$) and G-B ($R^2 = 0.13$, $R = -0.36$, $p < 0.05$) samples (Fig. S13e). Coupling between χ_{lf} and sediment mean grain size is generally weak in off G-B and P-S samples, but showed distinct groupings (Fig. S13).

4.5. Magnetic granulometry and optical microscopy on sieved sediment fractions

Magnetic granulometry data provided robust understanding on the sediment mixing, sorting and depositional processes in the shelf systems. The magnetite content showed good covariation with particle size. A systematic decrease in χ_{lf} with increasing particle size is noticed in all three shelf sediment cores (Fig. S14a, S14b, S14c). Samples off NTMS and G-B shelf displayed broad range in the distribution of magnetic particles within clastic grain size fractions. In general, magnetic granulometry results indicate that ferrimagnetic minerals preferentially reside in the silt and clay size fractions. Higher amount of magnetic particles were mainly contained in fine silt (4–20 μm), medium silt (20–40 μm) and clay fractions in NTMS and G-B samples (Fig. S14). Contrastingly, highest values of χ_{lf} were found to be confined in narrow (fine silt and clay) particle size range (Fig. S14).

Magnetic grain size diagnostic proxy (ARM/SIRM) showed good coupling with clastic grain size in all three cores (Fig. S14j, S14k, S14l). A systematic rise in magnetic grain size with increase in clastic grain size from 4 μm to 20 μm followed by near-stable values between 20 μm to 40 μm is noticed (Fig. S14j, S14k, S14l). We observed that this relationship reverses above > 40 μm (NTMS and G-B) and > 20 μm (P-S). In P-S samples, finer magnetic particles are found to be concentrated in the coarse silt (40 – 63 μm) and sand (>63 μm) fractions as seen through higher ARM/SIRM values (Fig. S14l). These results imply that 20 μm and 40 μm appears to be a threshold size limit above which ARM/SIRM ratio has limitation and cannot be further utilized as a magnetic grain-size diagnostic proxy. Occurrence of finer magnetic particles in >63 μm clastic grains as indicated by high ARM/SIRM (Fig. S14j, S14k, S14l) values in G-B and P-S samples could be attributed to the presence of finer magnetic inclusions within silicate grains (Hounslow and Maher, 1996; Hatfield, 2014).

In general, magnetic mineralogy diagnostic proxy (S-ratio) varied between 0.73 to 0.99 in all sediment core samples. Higher values of S-ratio and χ_{lf} in size fractions upto 63 μm in NTMS and 20 μm in P-S samples is indicative of the dominance of ferrimagnetic particles, which mostly resides in

the clay and fine silt fractions (Fig. S14g, S14i). In contrast, relatively lower and large fluctuation in S-ratio values of G-B samples suggest the dominance of both ferri- and antiferromagnetic particles (Fig. S14h). Average contribution of each magnetic particle size fraction towards the bulk sediment magnetic signal in NTMS, P-S and G-B samples are displayed in Fig. S15. NTMS sediments exhibited highest χ_{lf} values compared to P-S and G-B sediments. A systematic decrease in average magnetite concentration with increasing clastic grain size is clearly evident in all sediment cores (Fig. S15). In NTMS samples, χ_{lf} is predominantly governed by discrete magnetic particles contained in all clastic grain size fractions (Fig. S15). In P-S and G-B samples, clay (<4 μm) and fine-medium silt (4 μm - 40 μm) size magnetic particles are the major contributor to the bulk magnetic signal, while fraction > 40 μm had a negligible influence (Fig. S15). Optical microscopy on the sand (>63 μm) fraction of all three sediment cores indicated the presence of nanometre-sized magnetic particles embedded within silicate mineral grain (Fig. S16).

5. Discussion

5.1. Controls on the dispersal and deposition of magnetic minerals along the ECMI and WCMI: Evidences from rock magnetism, mineralogy and sedimentary records.

Sedimentary magnetic minerals record a wide range of geological processes and provide vital information on the provenance, climate induced weathering and erosional processes in the source areas and hydrodynamic regime at the marine sink (Oldfield et al., 1985; Liu et al., 2012; Roberts, 2015). Hence the knowledge on the composition (concentration, grain size, mineralogy) of magnetic minerals is prerequisite for the interpretation of rock magnetic and mineralogical records of shelf sediments (Liu et al., 2012). In this section, we discuss the potential factors controlling the dispersal and deposition of magnetic particles (derived from multiple sources) in the shelf system.

5.1.1. Contrasting sediment sources and climatic conditions

Rock magnetic records of the sediment cores from the shelf off NTMS, G-B and P-S display significant variation mainly in terms of magnetite content, mineralogy and grain size (Figs. 2, 3, 4) which can be linked to the changing sediment provenance controlled by the contrasting lithology, climatic conditions in the source region and changing hydraulic regime at each studied site (Fig. 1). The NTMS, P-S and G-B river systems deliver abundant magnetite-rich sediment load to the shelf (ECMI and WCMI), which are mainly derived from the DcB, APGC, Cuddappah Super Group (metamorphic, sedimentary) and Himalayan rocks (Quaternary sediments, Proterozoic sedimentary rocks, complex metamorphic and sedimentary sequences) (Kolla et al. 1981; Prins et al. 2000; Ramakrishnan and Vaidyanathan, 2010; Cai et al., 2020). As revealed by rock magnetism (remanence

parameters and χ -T curves), SEM-EDS and XRD data, magnetite, titanomagnetite and titanohematite particles of varying size and concentration are the dominant ferrimagnetic minerals in the studied sediments (Figs. 2, 3, 4, 5, 6, 7, 8, 9, 10).

Magnetite content in NTMS (5.27-7.22 wt %) and P-S (0.14-1.57 wt %) sediments are relatively higher compared to G-B sediments which varies between (0.37-0.58 wt %; Table. 2). A clear trend of decrease in magnetite content from NTMS to P-S to G-B shelf can be attributed to prominent change in magnetic mineral contribution from DcB to APGC, metamorphic and sedimentary rock dominated sediment province (Figs. 2, 3, 4, S15; Table 2). Highest magnetite content followed by consistently high S-ratio values (Fig. 2a, 2d) in NTMS samples suggest the predominance of detrital magnetic (ferrimagnetic) minerals which have undergone mere exposure to subaerial chemical weathering. Such unaltered rock magnetic characteristics is indicative of igneous source-rock lithology. Presence of abundant titanomagnetite particles in SEM-EDS (Figs. 7, S1, S2, S3) data suggest the dominance of DcB sourced ferrimagnetic minerals in the NTMS sediments. Major down-core shift in magnetic grain size and magnetite content from Z-II to Z-III (i.e., from 123 cmbsf onwards, Fig. 2) in core (SSK-40/GC-07) off NTMS can be linked to the drastic change either in the weathering regime and erosional processes in the source region. A gradual down-core fining of magnetic particles followed by decline in χ_{lf} values in the lowermost sediment magnetic zone (Z-III; Fig. 2) can be attributed to the period of enhanced chemical weathering in the source region (Kissel et al., 2003; Sebastian et al., 2019a). As we do not directly compare the magnetic signature of shelf sediments with the source-rock composition, a focussed isotopic and geochemical study on the dated sediment cores off NTMS is further warranted to precisely evaluate the role of monsoon-controlled source area weathering and erosional processes on the shelf sediment magnetic (content, grain size) record.

The G-B basin represents a network of complex river systems manifested by diverse physiography, catchment geologies, discharge, sediment load and experiences varying climatic conditions (Subramanian and Ramanathan, 1996; Whitehead et al., 2018). A distinct shift in magnetite content at ~ 110 cmbsf (Fig. 3a) accompanied by abrupt fluctuations in physical grain size (Fig. 3f) from 101 cmbsf to 128 cmbsf in core SSK-35/GC-14 off G-B shelf indicate marked change in detrital sedimentation pattern which is most likely controlled by changes in the differential contribution of source (*mafic versus felsic*) material. Compared to NTMS and P-S, the samples from G-B possessed lowest χ_{lf} values, but exhibit large scattering in the magnetic grain size (ARM/SIRM; Fig. 3). Such variability can be very-well attributed to the heterogeneity of the catchment geologies,

morphologies and differential sediment fluxes supplied by the tributaries which generated high compositional diversity in the basin sediments which gets regularly transported to the shelf region.

In marine sedimentary system, rock magnetic records has been successfully interpreted to infer the changes in weathering and erosional processes in the source region due to climatic shifts and tectonic processes (Colin et al., 1998; Evan and Heller, 2003; Kissel et al., 2003; Sebastian et al., 2019b; Damodararao et al., 2016; Miriyala et al., 2017). Off P-S shelf, a systematic pattern of down-core variation in magnetite content, grain size and mineralogy in sediment core SSK-50/GC-14 provided important insights into the source-to-sink related processes. For instance, high χ_{if} , SIRM and S-ratio values recorded in Z-I and Z-III of core SSK-50/GC-14 could be attributed to the period of enhanced supply of detrital (ferrimagnetic) particles to the shelf off P-S (Fig. 4a, 4c, 4d). A linkage between magnetic grain size proxy (ARM/SIRM) and weathering conditions in the source region has been well-established (Evan and Heller, 2003 Kissel et al., 2003; Sebastian et al., 2019a). Enhanced increase in the supply of fine-grained magnetic particles (as seen through elevated ARM/SIRM; Fig. 4a, 4e) manifested by high χ_{if} values in the uppermost sediment magnetic zone (Z-I) could be attributed to the period of increased chemical weathering in the source areas. Depleted χ_{if} and ARM/SIRM values suggest the presence of coarse-grained magnetic particles, which is most likely formed as a result of intense physical weathering (Sebastian et al., 2019a) in the source region.

Reduction in vegetation cover, increased physical erosion in the source areas could enhance the supply of highly coercive minerals in the terrigenous sediments (Phartiyal et al., 2003; Hu et al., 2020). Decline in χ_{if} and ARM/SIRM followed by consistent pattern of depleted S-ratio values in the lowermost sediment magnetic zone (Z-IV) of core SSK-50/GC-14 suggest the presence of highly coercive (titano hematite) and coarse-grained magnetic particles (Fig. 4a, 4d, 4e). As confirmed through SEM-EDS (Figs. 9, S9) and XRD (Fig. 10) data, increased proportion of titano hematite in Z-IV can be reconciled with the period of increased aridity in the source region (Derry and France-Lanord, 1996; Clift, 2017). Similar observations linking the presence of high coercive minerals with the aridity was reported from the Late Quaternary marine sediments off Gambia, NW Africa (Just et al., 2012a,b; Itambi et al., 2009) and Bengal Fan sediments (Abrajevitch et al., 2009)

5.1.2. Hydrodynamic control on bulk sediment magnetic properties

Complex hydrodynamic pattern on the continental shelves control the mixing, fractionation, settling and dispersal of magnetic particles (Gallaway et al., 2012; Hatfield, 2014). In addition to provenance and hydrodynamics, the concentration, grain size and mineralogy of magnetic particles is constrained by the drainage area, amount of sediment load, river length, littoral drift system, shelf

morphology and distance between river mouth and core location which can strongly modify the export of fluvial sediments to the marine sink (Razik et al., 2015). Shelf sediments off NTMS possess highest magnetite content (Table 2) and exhibit mere variations interms of magnetic mineralogy (Fig. 2). Such homogeneity in magnetic mineral composition suggests the dominance of DcB sourced material and the shelf sedimentation is predominantly constrained by fluvial (NTMS) plume. Magnetic grain size (ARM/SIRM) record of core SSK-40/GC-07 showed the presence of both fine as well as coarse-grained magnetic particles throughout the core, but exhibit distinct patterns (Fig. 2e). We put forward plausible explanation for the observed pattern. The larger sediment (DcB sourced, magnetite-rich) plume of mixed grain sizes generated by combined interaction of enhanced river runoffs and tidal currents extend to much larger area off NTMS shelf. It is highly possible that energetic estuarine-shelf transport system efficiently facilitated the dispersal of magnetic (fine and coarse grained) particles off NTMS shelf. Good coupling between magnetic susceptibility, magnetic crystal size and physical grain size (Fig. S13d, e) suggest that the transport of magnetic particles were predominantly driven by both bed as well as suspended load due to highly energetic fluvial (river runoff), and marine (tidal, waves) hydrodynamics which limited the density-based magnetic mineral sorting processes during source-to-sink transport.

Contrastingly, shelf sediments off G-B (SSK-35/GC-14) displayed much lower χ_{lf} values (Fig. 3a) and showed closed grouping (less variation) interms of magnetite content, but exhibit large scattering in the magnetic grain size (Figs. 3e, S13a, S13b) and mineralogy (Fig. 3d). Such variability can be attributed to the heterogeneity of the catchment geologies, morphologies, and differential sediment fluxes supplied by the tributaries of the G-B river system. High compositional diversity interms of mineralogy (Fig. 3d) and grain size (Figs. 6, S13b) in the regularly flushed G-B basin sediments is well-recorded in the shelf region. Fluvial sediment input and local hydrodynamics play a significant role in the evolution of the marine shelf sedimentation by controlling the sediment export to the nearshore and shelf region, but storage in terrestrial depocentres constrain the overall sediment movement from source-to-sink (Goodbred, 2003). Recent studies linked the time-varying decline in sediment flux delivered by G-B river system to the shelf region with the long term storage within Indo-Gangetic plain and basin (Joussain et al., 2017; Rahman et al., 2018), complex dispersal mechanism of sediment plume in the nearshore and shelf region (Chauhan et al., 2005), change in the morphology of the sediment routing system (Fournier et al., 2017; Haque et al., 2021), magnitude of fluvial flux of the G–B associated with monsoonal changes (Wasson, 2003; Joussain et al., 2017; Kumar et al., 2019), erosional rates linked with tectonic and geomorphological changes (Singh, 2006). Magnetic mineral grain size record reveal the dominance of fine-grained magnetic particles in

core SSK-35/GC-14 off G-B shelf (Fig. 3e). A mineral magnetic study by Panwar et al. (2020) in the upper catchment (Alaknanda and Ramganga rivers) area of the Ganga basin reported the presence of both fine and coarse-grained magnetic particles of mixed (ferri and antiferromagnetic) mineralogy derived from mafic and felsic rocks. The rock magnetic (Fig. 3) and mineralogy (Figs. 8, 10, S4, S5, S6) records of sediment core SSK-35/GC-14 off G-B revealed the presence of fine-grained magnetic particles of mixed magnetic (magnetite, titanomagnetite, titanohematite) mineralogies. We put forward following plausible scenario to explain the (a) plausible mechanism favouring the preferential enrichment of fine-grained magnetic particles off G-B shelf and (b) decline in abundance of coarser magnetic particles exported out from the G-B basin settle inspite of higher shelf sedimentation. We hypothesize that the monsoon-controlled sediment partitioning regime within the G-B basin might have caused selective washout of finer magnetic particles of mixed magnetic mineralogy which obviously cannot permanently settle within the basin during high river run off and under the prevailing wave and tide conditions in deltaic and nearshore region and got further transported into the G-B shelf. Sorting and enrichment of fine-grained magnetic particles at shelf region of G-B by tidal and waves mixing is clearly mirrored by the relatively narrow and closed grouping interms of magnetic and physical (Fig. S13e).

The G-B river system delivers huge amount of sediments into the Bengal shelf, where tide-driven processes disperse the sediments on the shelf region. The sediment core is located on the western site of the wide deep shelf canyon (Swatch of No Ground (SoNG); Michels et al., 2003; Kudrass et al., 2018; Fig. 1) that deeply incises the Bengal shelf near the Ganges–Brahmaputra river mouth, and acts as a potential sediment conduit for the transport of riverine sediments between G-B river mouth and Bengal Fan. Sediment magnetism, physical properties and clay mineralogy based studies highlighted that SoNG interrupts the along and across-shelf transport of riverine sediments (Segall and Kuehl 1992; Sebastian et al., 2019a). Previous study linked the absence of fine-grained sediments in the canyon with the gravity-driven low density currents, which preferentially inhibited the deposition of fine sediments in the main channel of SoNG. Magnetic (Fig. 3e) and physical (Fig. 3f) grain size record of core SSK-35/GC-14 off G-B shelf revealed the lack of coarser and dominance of fine-grained magnetic as well as clastic grain size particles. It is highly possible that SoNG acted as a trap for the coarse-grained magnetic particles delivered by the G-B rivers systems, which gets preferentially transported as bedload from the shelf to the Bengal fan. Concurrently, the finer magnetic particles most likely remain as suspended load for longer period due to higher tidal and wave energies at the G-B river mouth, gets dispersed away from the SoNG and further remain deposited on the shelf due to differential sediment partitioning regime. Good coupling ($R = -0.36$,

$p < 0.05$) between magnetic and clastic grain size in G-B samples (Fig. S13e) provide evidence on the efficient sediment sorting process at SoNG and preferential transport and deposition of fine-grained magnetic particles at western side (core location) of the G-B shelf (Fig. 1b).

Apparent mixing of sediments derived from diverse lithologies (DCB, APGC, and Cuddappah Super Group rocks) along WCMI and ECMI can induce distinct magnetic signature, which can be easily detected from mineralogy diagnostic magnetic proxy. As the dominant net littoral drift system is south-westerly directed along the ECMI the sediment contribution from the Krishna-Godavari (DcB sourced) river systems in the study area via longshore sediment transport can be significant (Chandramohan and Nayak, 1991; Kumar et al., 2006; Bejugam and Nayak, 2017). A clear shift in S-ratio from 177 cmbsf onwards marks the onset of DcB sourced material in the shelf sediments off P-S (Fig. 4d). Presence of abundant titanomagnetite in varying proportion from Z-III to Z-I in core off P-S shelf (SSK-50/GC-14) reflects the increased contributions from basaltic (DcB) terrains off P-S shelf delivered via longshore sediment transport system. The successive mixing of sediments off P-S shelf derived from P-S hinterland (sedimentary and metamorphic) and alongshore transported DcB material from Krishna and Godavari shelf is clearly expressed by elongated, slightly curvilinear and large spreading in the bivariate plot of concentration dependent magnetic parameters (Fig. S13a). Synchronized increase in physical (Fig. 4f) and magnetic (Fig. 4e) grain size coupled with marked decrease in magnetite content (Fig. 4a) between 45 – 92 cmbsf in core SSK-50/GC-14 can be linked with the period representing rapid perturbation in detrital sedimentation.

5.2. Response of different sized magnetic particles to shelfal sediment dynamics (mixing, sorting, settling), and post-depositional processes.

Magnetic particles are transported to the continental shelf region of the studied sites from Arabian Sea (SSK-40/GC-07) and Bay of Bengal (SSK-35/GC-14; SSK-50/GC-14) mainly by NTMS, G-B and P-S river systems. Mixing, fractionation, transport and settling of magnetic particles at the studied sites are largely governed by bulk sediment composition (grain size, mineral density) and the strong interaction between tidal currents, bathymetry, waves and alongshore littoral drift system (WICC, EICC; Shankar et al., 2002). Grain size of magnetic minerals has a pronounced impact on the sediment magnetism in addition to magnetic mineralogy (Liu et al., 2012). The magnetogranulometric signatures of three sediment cores (Figs. S14, S15) has been evaluated to understand how different size magnetic particles derived from wide array of source regions respond to shelfal sedimentary (mixing, fractionation, settling) processes. A systematic decline in average magnetite content with increase in clastic grain size is observed in P-S and G-B samples (Fig. S15). Contrastingly, relatively high and stable magnetite content persist in all clastic grain size fractions of

NTMS samples (Fig. S15). Comparing the contribution of individual grain size fraction towards bulk sediment signal, it is clearly evident that clay and silt ($< 40 \mu\text{m}$; fine and medium) fraction carry higher magnetite content in G-B and P-S samples, while in NTMS samples all size fractions (sand, silt, clay) contribute substantially to the bulk sediment magnetic signal (Fig. S15). Such a non-covariation exhibiting differential contribution from individual magnetic fractions towards the bulk signal imply the control of both provenance as well as transport dynamics on the bulk sediment magnetic signal. For example in core off NTMS (SSK-40/GC-07), abundant supply of different size magnetic particles (igneous origin) followed by intense mixing due to weaker sediment partitioning regime within estuaries and shelf probably resulted in the uniform distribution of magnetic particles in all clastic size fractions and reflect provenance control (Fig. S15). This observation imply that grain size and mineral density selective fractionation of magnetic particles during transport and deposition had a negligible impact on magnetic source characteristics of NTMS samples. The dispersal and deposition of magnetic particles off G-B shelf is strongly modulated by the presence of submarine canyon (SoNG) and wave dynamics, which efficiently sorted and dispersed the fine-grained magnetic particles towards core location (SSK-35/GC-14) and thereby enriched coarser particles within SoNG. The sorting and dispersal process is clearly mirrored in the magnetogranulometry data, where higher magnetite content was mainly contained in the clay and fine silt fraction of core off G-B shelf (Fig. S15). A trend of systematic decline in magnetite content with increase in clastic grain size of G-B samples (Fig. S15) suggest that most of the coarse grained magnetic particles ($> 40 \mu\text{m}$) predominantly remained trapped within SoNG and does not reach the core site (SSK-35/GC-14).

Sedimentary magnetic minerals can occur as discrete as well as inclusions within polycrystalline clasts in marine sediments (Hatfield, 2014; Razik et al., 2014). Ferrimagnetic particles in volcanic, igneous and metamorphic rocks can occur in different grain sizes (Hounslow and Maher, 1996; Hatfield et al., 2014). Fine-grained magnetic particles occurring as inclusions within silicates are widespread and has been widely reported from estuarine and marine sediments for example in shelf sediments off New Zealand (Badesab et al., 2017), shelf off NE Australia (Maher et al., 2009), shelf off NW Africa (Razik et al., 2014), South American continental margin (Razik et al., 2015), North Atlantic (Hatfield et al., 2014; 2017), and Japan Sea (Chang et al., 2016). Magnetogranulometry data revealed that magnetic grain size is independent of physical grain size above $>20 \mu\text{m}$ in P-S (Fig. S14l) and above $>40 \mu\text{m}$ in NTMS (Fig. S14j) and G-B (Fig. S14k) samples. Decoupling between magnetic and physical grain size (Fig. S14) could be linked with polycrystallinity and explain the reason for the occurrence of finer magnetic particles as inclusions in

silt and sand fractions as evident through slight increase in ARM/SIRM and χ_{lf} values (Fig. S14a, S14b, S14c, S14j, S14k, S14l; Hatfield et al., 2014). The optical microscopy of $>63 \mu\text{m}$ fractions (Fig. S16) representing different depth intervals of the studied sediment cores confirmed the presence of fine-grained magnetic particles occurring as inclusions in large clastic grain size fractions and therefore explain the reason for high ARM/SIRM and χ_{lf} $>63 \mu\text{m}$ fractions (Fig. S14a, S14b, S14c, S14j, S14k, S14l).

Post-depositional processes including reductive diagenesis (dissolution of detrital iron oxides), authigenesis (precipitation of ferrimagnetic iron sulfides) and biogenesis (bacterial biomineralization of ultrafine magnetite) can strongly modify the primary magnetic mineral assemblages in marine sediments (Karlín and Levi, 1985; Roberts, 2015). We did not observe any significant presence of magnetic iron sulfides in SEM-EDS and XRD data of all analyzed samples except in Z-IV (Fig. 4) of core SSK-50/GC-14 off shelf P-S, which showed the presence of diagenetically formed pyrite. Delineating the magnetic signatures linked with diagenetic, authigenic and biogenic processes was not the major focus and beyond the scope of this work. Moreover, a dedicated investigation involving organic and pore-water geochemistry is further warranted to precisely evaluate the postdepositional influences on the sediment magnetic signal.

6. Conclusions

The present study systematically evaluated the impact of contrasting provenance and shelfal sediment dynamics on the sediment magnetic properties. Variability in magnetic mineral composition (content, grain size, mineralogy) and clastic grain size distribution in shelfal sediments is closely linked with the provenance changes, differential sediment contribution and site-specific hydro-and sediment dynamics. The findings of this study are summarized below:

(1) Magnetite, titanomagnetite, titanohematite particles of detrital origin, with variable concentration and grain sizes (SD-PSD-MD) constitute the bulk magnetic mineralogy of the shelf sediments. A clear trend of decrease in magnetite content from NTMS to P-S to G-B shelf can be attributed to enhanced change in magnetic mineral contribution from DcB to APGC, metamorphic and sedimentary rock dominated sediment province. A distinct shift in magnetite content accompanied by abrupt fluctuations in clastic grain size in core off G-B shelf indicate the marked change in detrital sedimentation pattern. A systematic pattern of down-core variation in magnetite content, grain size and mineralogy in the sediment core off P-S shelf, provided valuable insights into the source-to-sink related processes. A major shift in mineralogy diagnostic proxy (S-ratio) marked the onset of DcB sourced material in the shelf sediments off P-S.

(2) Magnetic measurement of specific size sediment fractions permitted isolation and targeting of certain magnetic characteristic for discriminating changes in sediment provenance and depositional regime. Magnetogranulometry and optical microscopy data revealed that decoupling between magnetic crystal and physical grain size in NTMS and G-B (>40 μm), and P-S (>20 μm) shelf sediments is mainly be linked with the polycrystalline nature, where fine-grained magnetic particles occurred as inclusions within silt and sand fractions.

(3) The present study demonstrated that integrated approach combining rockmagnetic, mineralogical and sedimentological methods can be effectively used to elucidate the influence of the contrasting provenance and oceanographic conditions on the dispersal and deposition of magnetic particle in the shelf systems.

Declaration of competing interest

The authors declare that they have no known competing financial interests or personal relationships that could have appeared to influence the work reported in this paper.

Acknowledgement

We thank the Director, CSIR–NIO for supporting this study. We acknowledge the support of the project members and the ship cell personnel of CSIR-NIO for providing assistance in collection of sediment cores during the scientific expeditions (of project GEOSINKS- CSIR XII Plan projects GEOSINKS (PSC0106) of research vessel R/V Sindhu Sankalp of CSIR-NIO. We thank the Director of the CSIR-National Geophysical Research Institute (NGRI), Hyderabad, India for providing access to the Paleomagnetic laboratory. NBK is thankful to the Council of Scientific and Industrial Research, India for providing Junior Research Fellowship. We thank Girish Prabhu and Areef Sardar for providing assistance with XRD and SEM-EDS analyses at CSIR-NIO respectively. We thank Dr. Mandar Nanajkar for his assistance with optical microscopy. Thanks to Omkar Naikgaonkar and Prem Piyush Panda for providing assistance with sub-sampling of sediment cores. We thank Dr. John Kurian for providing assistance with the grain size analyses at NCPOR, Goa, India. The data used in this study is available on CSIR-NIO repository. The link to access data online is <https://publication-data.nio.org/s/bedo7Be7Dngzm9y>.

References

- Abrajevitch, A., der Voo, R. van, Rea, D.K., 2009. Variations in relative abundances of goethite and hematite in Bengal Fan sediments: Climatic vs. diagenetic signals. *Marine Geology* 267, 191–206. <https://doi.org/10.1016/j.margeo.2009.10.010>
- Alagarsamy, R., 2009. Environmental magnetism and application in the continental shelf sediments of India. *Marine Environmental Research* 68 (2), 49–58. <https://doi.org/10.1016/j.marenvres.2009.04.003>
- Amiel, N., Shaar, R., Sivan, O., 2020. The Effect of Early Diagenesis in Methanic Sediments on Sedimentary Magnetic Properties: Case Study From the SE Mediterranean Continental Shelf. *Frontiers in Earth Science* 8. <https://doi.org/10.3389/feart.2020.00283>
- Anand, M., 2003. Early Proterozoic Melt Generation Processes beneath the Intra-cratonic Cuddapah Basin, Southern India. *Journal of Petrology* 44, 2139–2171. <https://doi.org/10.1093/petrology/egg073>
- Badesab, F., von Dobeneck, T., Briggs, R.M., Bryan, K.R., Just, J., Müller, H., 2017. Sediment dynamics of an artificially deepened mesotidal coastal lagoon: An environmental magnetic investigation of Tauranga Harbour, New Zealand. *Estuarine, Coastal and Shelf Science* 194, 240–251. <https://doi.org/10.1016/j.ecss.2017.06.017>
- Bejugam, P., Nayak, G.N., 2017. Source and depositional processes of the surface sediments and their implications on productivity in recent past off Mahanadi to Pennar River mouths, western Bay of Bengal. *Palaeogeography, Palaeoclimatology, Palaeoecology* 483, 58–69. <https://doi.org/10.1016/j.palaeo.2016.12.006>
- Bloemendal, J., King, J.W., Hall, F.R., Doh, S.J., 1992. Rock magnetism of Late Neogene and Pleistocene deep-sea sediments: Relationship to sediment source, diagenetic processes, and sediment lithology. *Journal of Geophysical Research: Solid Earth* 97(B4), 4361–4375. <https://doi.org/10.1029/91JB03068>
- Cai, M., Xu, Z., Clift, P.D., Khim, B.-K., Lim, D., Yu, Z., Kulhanek, D.K., Li, T., 2020. Long-term history of sediment inputs to the eastern Arabian Sea and its implications for the evolution of the Indian summer monsoon since 3.7 Ma. *Geological Magazine* 157, 908–919. <https://doi.org/10.1017/S0016756818000857>
- Caricchi, C., Lucchi, R.G., Sagnotti, L., Macrì, P., Morigi, C., Melis, R., Caffau, M., Rebesco, M., Hanebuth, T.J.J., 2018. Paleomagnetism and rock magnetism from sediments along a continental shelf-to-slope transect in the NW Barents Sea: Implications for geomagnetic and depositional changes during the past 15 thousand years. *Global and Planetary Change* 160, 10–27. <https://doi.org/10.1016/j.gloplacha.2017.11.007>
- Chandramohan, P., Nayak, B.U., 1991. Longshore sediment transport along the Indian coast. *Indian Journal of Marine Sciences* 20, 110–114.
- Chang, L., Bolton, C.T., Dekkers, M.J., Hayashida, A., Heslop, D., Krijgsman, W., Kodama, K., Paterson, G.A., Roberts, A.P., Rohling, E.J., Yamamoto, Y., Zhao, X., 2016. Asian monsoon modulation of nonsteady state diagenesis in hemipelagic marine sediments offshore of Japan. *Geochemistry, Geophysics, Geosystems* 17, 4383–4398. <https://doi.org/10.1002/2016GC006344>

- Chauhan, O.S., Rajawat, A.S., Pradhan, Y., Suneethi, J., Nayak, S.R., 2005. Weekly observations on dispersal and sink pathways of the terrigenous flux of the Ganga–Brahmaputra in the Bay of Bengal during NE monsoon. *Deep Sea Research Part II: Topical Studies in Oceanography* 52, 2018–2030. <https://doi.org/10.1016/j.dsr2.2005.05.012>
- Chiocci, F.L., Chivas, A.R., 2014. Chapter 1 An overview of the continental shelves of the world. Geological Society, London, *Memoirs* 41, 1–5. <https://doi.org/10.1144/M41.1>
- Clift, P.D., 2017. Cenozoic sedimentary records of climate-tectonic coupling in the Western Himalaya. *Progress in Earth and Planetary Science* 4(1), 1–22. <https://doi.org/10.1186/s40645-017-0151-8>
- Coleman, J.M., 1969. Brahmaputra river: Channel processes and sedimentation. *Sedimentary Geology* 3, 129–239. [https://doi.org/10.1016/0037-0738\(69\)90010-4](https://doi.org/10.1016/0037-0738(69)90010-4)
- Colin, C., Kissel, C., Blamart, D., Turpin, L., 1998. Magnetic properties of sediments in the Bay of Bengal and the Andaman Sea: impact of rapid North Atlantic Ocean climatic events on the strength of the Indian monsoon. *Earth and Planetary Science Letters* 160, 623–635. [https://doi.org/10.1016/S0012-821X\(98\)00116-2](https://doi.org/10.1016/S0012-821X(98)00116-2)
- Cruz, A.P.S., Barbosa, C.F., Ayres-Neto, A., Munayco, P., Scorzelli, R.B., Amorim, N.S., Albuquerque, A.L.S., Seoane, J.C.S., 2018. Geochemistry and magnetic sediment distribution at the western boundary upwelling system of southwest Atlantic. *Continental Shelf Research* 153, 64–74. <https://doi.org/10.1016/j.csr.2017.12.011>
- Cui, M., Wang, Z., Nageswara Rao, K., Sangode, S.J., Saito, Y., Chen, T., Kulkarni, Y.R., Naga Kumar, K.C.V. and Demudu, G., 2017. A mid-to late-Holocene record of vegetation decline and erosion triggered by monsoon weakening and human adaptations in the south-east Indian Peninsula. *The Holocene* 27(12), 1976–1987. <https://doi.org/10.1177/0959683617715694>
- Damodararao, K., Singh, S.K., Rai, V.K., Ramaswamy, V. and Rao, P.S., 2016. Lithology, monsoon and sea-surface current control on provenance, dispersal and deposition of sediments over the Andaman continental shelf. *Frontiers in Marine Science* 3, p.118. <https://doi.org/10.3389/fmars.2016.00118>
- Dash, C., Shankar, R., Pati, P., Jose, J., Seong, Y.B., Dhal, S.P., Manjunatha, B.R. and Sandeep, K., 2022. An environmental magnetic record of Holocene climatic variability from the Chilika Lagoon, Southern Mahanadi Delta, east coast of India. *Journal of Asian Earth Sciences* 230, 105190. <https://doi.org/10.1016/j.jseaes.2022.105190>
- Day, R., Fuller, M., Schmidt, V.A., 1977. Hysteresis properties of titanomagnetites: Grain-size and compositional dependence. *Physics of the Earth and Planetary Interiors* 13, 260–267. [https://doi.org/10.1016/0031-9201\(77\)90108-X](https://doi.org/10.1016/0031-9201(77)90108-X)
- DeCelles, P.G., Robinson, D.M., Quade, J., Ojha, T.P., Garzione, C.N., Copeland, P., Upreti, B.N., 2001. Stratigraphy, structure, and tectonic evolution of the Himalayan fold-thrust belt in western Nepal. *Tectonics* 20, 487–509. <https://doi.org/10.1029/2000TC001226>
- Derry, L.A., France-Lanord, C., 1996. Neogene Himalayan weathering history and river⁸⁷Sr⁸⁶Sr: impact on the marine Sr record. *Earth and Planetary Science Letters* 142, 59–74. [https://doi.org/10.1016/0012-821X\(96\)00091-X](https://doi.org/10.1016/0012-821X(96)00091-X)

- Dunlop, D.J., 2002. Theory and application of the Day plot (M_{rs} / M_s versus H_{cr} / H_c) 2. Application to data for rocks, sediments, and soils. *Journal of Geophysical Research* 107, 2057. <https://doi.org/10.1029/2001JB000487>
- Dunlop, D.J., Özdemir, Ö., 1997. *Rock Magnetism*. Cambridge University Press. <https://doi.org/10.1017/CBO9780511612794>
- Evans, M.E., Heller, F., 2003. *Environmental Magnetism: Principles and Applications of Enviromagnetics*. Academic Press, San Diego.
- Fournier, L., Fauquembergue, K., Zaragosi, S., Zorzi, C., Malaizé, B., Bassinot, F., Jousain, R., Colin, C., Moreno, E., Leparmentier, F., 2017. The Bengal fan: External controls on the Holocene Active Channel turbidite activity. *The Holocene* 27, 900–913. <https://doi.org/10.1177/0959683616675938>
- Gallaway, E., Trenhaile, A.S., Cioppa, M.T. and Hatfield, R.G., 2012. Magnetic mineral transport and sorting in the swash-zone: northern Lake Erie, Canada. *Sedimentology* 59(6), 1718–1734. <https://doi.org/10.1111/j.1365-3091.2012.01323.x>
- Gao, S., Collins, M.B., 2014. Holocene sedimentary systems on continental shelves. *Marine Geology* 352, 268–294. <https://doi.org/10.1016/j.margeo.2014.03.021>
- Garzanti, E., 1999. Stratigraphy and sedimentary history of the Nepal Tethys Himalaya passive margin. *Journal of Asian Earth Sciences* 17, 805–827. [https://doi.org/10.1016/S1367-9120\(99\)00017-6](https://doi.org/10.1016/S1367-9120(99)00017-6)
- Garzanti, E., Vezzoli, G., Andò, S., Limonta, M., Borromeo, L., France-Lanord, C., 2019. Provenance of Bengal Shelf Sediments: 2. Petrology and Geochemistry of Sand. *Minerals* 9, 642. <https://doi.org/10.3390/min9100642>
- Ge, C., Zhang, W., Dong, C., Dong, Y., Bai, X., Liu, J., Hien, N.T.T., Feng, H., Yu, L., 2015. Magnetic mineral diagenesis in the river-dominated inner shelf of the East China Sea, China. *Journal of Geophysical Research: Solid Earth* 120, 4720–4733. <https://doi.org/10.1002/2015JB011952>
- Goodbred, S.L., 2003. Response of the Ganges dispersal system to climate change: a source-to-sink view since the last interstade. *Sedimentary Geology* 162, 83–104. [https://doi.org/10.1016/S0037-0738\(03\)00217-3](https://doi.org/10.1016/S0037-0738(03)00217-3)
- Gupta, H., Chakrapani, G.J., 2005. Temporal and spatial variations in water flow and sediment load in Narmada River Basin, India: natural and man-made factors. *Environmental Geology* 48, 579–589. <https://doi.org/10.1007/s00254-005-1314-2>
- Haque, S., Ali, Md.M., Islam, A.K.M.S., Khan, J.U., 2021. Changes in flow and sediment load of poorly gauged Brahmaputra river basin under an extreme climate scenario. *Journal of Water and Climate Change* 12, 937–954. <https://doi.org/10.2166/wcc.2020.219>
- Hatfield, R., 2014. Particle Size-Specific Magnetic Measurements as a Tool for Enhancing Our Understanding of the Bulk Magnetic Properties of Sediments. *Minerals* 4, 758–787. <https://doi.org/10.3390/min4040758>

- He, K., Zhao, Xiangyu, Pan, Y., Zhao, Xiang, Qin, H., Zhang, T., 2020. Benchmarking Component Analysis of Remanent Magnetization Curves With a Synthetic Mixture Series: Insight Into the Reliability of Unmixing Natural Samples. *Journal of Geophysical Research: Solid Earth* 125. <https://doi.org/10.1029/2020JB020105>
- Hirt, A.M., Gehring, A.U., 1991. Thermal alteration of the magnetic mineralogy in ferruginous rocks. *Journal of Geophysical Research* 96, 9947. <https://doi.org/10.1029/91JB00573>
- Hounslow, M.W., Maher, B.A., 1996. Quantitative extraction and analysis of carriers of magnetization in sediments. *Geophysical Journal International* 124, 57–74. <https://doi.org/10.1111/j.1365-246X.1996.tb06352.x>
- Hu, P., Heslop, D., Rossel, R.A.V., Roberts, A.P. and Zhao, X., 2020. Continental-scale magnetic properties of surficial Australian soils. *Earth-Science Reviews*, 203, p.103028. <https://doi.org/10.1016/j.earscirev.2019.103028>
- Itambi, A.C., von Dobeneck, T., Mulitza, S., Bickert, T. and Heslop, D., 2009. Millennial-scale northwest African droughts related to Heinrich events and Dansgaard-Oeschger cycles: Evidence in marine sediments from offshore Senegal. *Paleoceanography* 24(1). <https://doi.org/10.1029/2007PA001570>
- Joussain, R., Liu, Z., Colin, C., Duchamp-Alphonse, S., Yu, Z., Moréno, E., Fournier, L., Zaragosi, S., Dapoigny, A., Meynadier, L., Bassinot, F., 2017. Link between Indian monsoon rainfall and physical erosion in the Himalayan system during the Holocene. *Geochemistry, Geophysics, Geosystems* 18, 3452–3469. <https://doi.org/10.1002/2016GC006762>
- Just, J., Dekkers, M.J., von Dobeneck, T., van Hoesel, A., Bickert, T., 2012a. Signatures and significance of aeolian, fluvial, bacterial and diagenetic magnetic mineral fractions in Late Quaternary marine sediments off Gambia, NW Africa. *Geochemistry, Geophysics, Geosystems* 13. <https://doi.org/10.1029/2012GC004146>
- Just, J., Heslop, D., von Dobeneck, T., Bickert, T., Dekkers, M.J., Frederichs, T., Meyer, I. and Zabel, M., 2012. Multiproxy characterization and budgeting of terrigenous end-members at the NW African continental margin. *Geochemistry, Geophysics, Geosystems* 13(9). <https://doi.org/10.1029/2012GC004148>
- Karlin, R. and Levi, S., 1985. Geochemical and sedimentological control of the magnetic properties of hemipelagic sediments. *Journal of Geophysical Research: Solid Earth* 90(B12), 10373–10392. <https://doi.org/10.1029/JB090iB12p10373>
- Kissel, C., Laj, C., Clemens, S., Solheid, P., 2003. Magnetic signature of environmental changes in the last 1.2 Myr at ODP Site 1146, South China Sea. *Marine Geology* 201, 119–132. [https://doi.org/10.1016/S0025-3227\(03\)00212-3](https://doi.org/10.1016/S0025-3227(03)00212-3)
- Kissel, C., Liu, Z., Li, J., Wandres, C., 2016. Magnetic minerals in three Asian rivers draining into the South China Sea: Pearl, Red, and Mekong Rivers. *Geochemistry, Geophysics, Geosystems* 17, 1678–1693. <https://doi.org/10.1002/2016GC006283>
- Kolla, V., Kostecki, J.A., Robinson, F., Biscaye, P.E. and Ray, P.K., 1981. Distributions and origins of clay minerals and quartz in surface sediments of the Arabian Sea. *Journal of Sedimentary Research*, 51(2), 563–569. <https://doi.org/10.1306/212F7CD9-2B24-11D7-8648000102C1865D>

- Kudrass, H.R., Machalett, B., Palamenghi, L., Meyer, I., Zhang, W., 2018. Sediment transport by tropical cyclones recorded in a submarine canyon off Bangladesh. *Geo-Marine Letters* 38, 481–496. <https://doi.org/10.1007/s00367-018-0550-x>
- Kulkarni, Y.R., Sangode, S.J., Meshram, D.C., Patil, S.K. and Dutt, Y., 2014. Mineral magnetic characterization of the Godavari river sediments: implications to Deccan basalt weathering. *Journal of the Geological Society of India* 83(4),376-384. <https://doi.org/10.1007/s12594-014-0054-x>
- Kumar, V., Gupta, V., Sundriyal, Y.P., 2019. Spatial interrelationship of landslides, litho-tectonics, and climate regime, Satluj valley, Northwest Himalaya. *Geological Journal* 54, 537–551. <https://doi.org/10.1002/gj.3204>
- Kumar, V.S., Pathak, K.C., Pednekar, P., Raju, N.S.N., Gowthaman, R., 2006. Coastal processes along the Indian coastline. *Current Science* 91, 530–536. <https://www.jstor.org/stable/24093957>
- Lattard, D., Engelmann, R., Kontny, A., Sauerzapf, U., 2006. Curie temperatures of synthetic titanomagnetites in the Fe-Ti-O system: Effects of composition, crystal chemistry, and thermomagnetic methods. *Journal of Geophysical Research: Solid Earth* 111, n/a-n/a. <https://doi.org/10.1029/2006JB004591>
- Liu, Q., Roberts, A.P., Larrasoana, J.C., Banerjee, S.K., Guyodo, Y., Tauxe, L., Oldfield, F., 2012. Environmental magnetism: Principles and applications. *Reviews of Geophysics* 50, RG4002. <https://doi.org/10.1029/2012RG000393>
- Maher, B.A., 1988. Magnetic properties of some synthetic sub-micron magnetites. *Geophysical Journal International* 94, 83–96. <https://doi.org/10.1111/j.1365-246X.1988.tb03429.x>
- Maher, B.A., Watkins, S.J., Brunskill, G., Alexander, J., Fielding, C.R., 2009. Sediment provenance in a tropical fluvial and marine context by magnetic ‘fingerprinting’ of transportable sand fractions. *Sedimentology* 56, 841–861. <https://doi.org/10.1111/j.1365-3091.2008.00999.x>
- Michels, K.H., Suckow, A., Breitzke, M., Kudrass, H.R., Kottke, B., 2003. Sediment transport in the shelf canyon “Swatch of No Ground” (Bay of Bengal). *Deep Sea Research Part II: Topical Studies in Oceanography* 50, 1003–1022. [https://doi.org/10.1016/S0967-0645\(02\)00617-3](https://doi.org/10.1016/S0967-0645(02)00617-3)
- Milliman, J.D., Meade, R.H., 1983. World-Wide Delivery of River Sediment to the Oceans. *The Journal of Geology* 91, 1–21. <https://doi.org/10.1086/628741>
- Miriyala, P., Sukumaran, N.P., Nath, B.N., Ramamurty, P.B., Sijinkumar, A.V., Vijayagopal, B., Ramaswamy, V. and Sebastian, T., 2017. Increased chemical weathering during the deglacial to mid-Holocene summer monsoon intensification. *Scientific reports* 7(1), 1-11. <https://doi.org/10.1038/srep44310>
- Nagai, R.H., Ferreira, P.A.L., Mulkherjee, S., Martins, M.V., Figueira, R.C.L., Sousa, S.H.M., Mahiques, M.M., 2014. Hydrodynamic controls on the distribution of surface sediments from the southeast South American continental shelf between 23°S and 38°S. *Continental Shelf Research* 89, 51–60. <https://doi.org/10.1016/j.csr.2013.09.016>

- Nowaczyk, N.R., 2011. Dissolution of titanomagnetite and sulphidization in sediments from Lake Kinneret, Israel. *Geophysical Journal International* 187, 34–44. <https://doi.org/10.1111/j.1365-246X.2011.05120.x>
- Oldfield, F., Maher, B.A., Donoghue, J. and Pierce, J., 1985. Particle-size related, mineral magnetic source sediment linkages in the Rhode River catchment, Maryland, USA. *Journal of the Geological Society* 142(6), 1035–1046. <https://doi.org/10.1144/gsjgs.142.6.1035>
- Pan, Y., Zhu, R., Banerjee, S.K., Gill, J., Williams, Q., 2000. Rock magnetic properties related to thermal treatment of siderite: Behavior and interpretation. *Journal of Geophysical Research: Solid Earth* 105, 783–794. <https://doi.org/10.1029/1999JB900358>
- Panda, D.K., Kumar, A., Mohanty, S., 2011. Recent trends in sediment load of the tropical (Peninsular) river basins of India. *Global and Planetary Change* 75, 108–118. <https://doi.org/10.1016/j.gloplacha.2010.10.012>
- Panwar, S., Yang, S., Srivastava, P., Khan, M.Y.A., Sangode, S.J., Chakrapani, G.J., 2020. Environmental magnetic characterization of the Alaknanda and Ramganga river sediments, Ganga basin, India. *CATENA* 190, 104529. <https://doi.org/10.1016/j.catena.2020.104529>
- Passier, H.F., de Lange, G.J., Dekkers, M.J., 2001. Magnetic properties and geochemistry of the active oxidation front and the youngest sapropel in the eastern Mediterranean Sea. *Geophysical Journal International* 145, 604–614. <https://doi.org/10.1046/j.0956-540x.2001.01394.x>
- Patel, P., Raju, N.J., Subramanian, V., Gossel, W., Wycisk, P., 2020. Chemical weathering and atmospheric CO₂ consumption in the semi-arid Swarnamukhi basin (Peninsular India) estimated from river water geochemistry. *Applied Geochemistry* 113, 104520. <https://doi.org/10.1016/j.apgeochem.2020.104520>
- Pepper, D.A., Stone, G.W., 2004. Hydrodynamic and sedimentary responses to two contrasting winter storms on the inner shelf of the northern Gulf of Mexico. *Marine Geology* 210, 43–62. <https://doi.org/10.1016/j.margeo.2004.05.004>
- Petersen, N., von Dobeneck, T., Vali, H., 1986. Fossil bacterial magnetite in deep-sea sediments from the South Atlantic Ocean. *Nature* 320, 611–615. <https://doi.org/10.1038/320611a0>
- Phartiyal, B., Appel, E., Blaha, U., Hoffmann, V., Kotlia, B.S., 2003. Palaeoclimatic significance of magnetic properties from Late Quaternary lacustrine sediments at Pithoragarh, Kumaun Lesser Himalaya, India. *Quaternary International* 108, 51–62. [https://doi.org/10.1016/S1040-6182\(02\)00193-3](https://doi.org/10.1016/S1040-6182(02)00193-3)
- Philips, S. C., 2018. Diagenetic degradation of paleoenvironmental signals in magnetic susceptibility in the northern Bay of Bengal, *The IRM Quarterly*, Winter 2017-2018, Vol. 27 No.4
- Prins, M.A., Postma, G., Cleveringa, J., Cramp, A., Kenyon, N.H., 2000. Controls on terrigenous sediment supply to the Arabian Sea during the late Quaternary: the Indus Fan. *Marine Geology* 169, 327–349. [https://doi.org/10.1016/S0025-3227\(00\)00086-4](https://doi.org/10.1016/S0025-3227(00)00086-4)

- Rahman, M., Dustegir, M., Karim, R., Haque, A., Nicholls, R.J., Darby, S.E., Nakagawa, H., Hossain, M., Dunn, F.E., Akter, M., 2018. Recent sediment flux to the Ganges-Brahmaputra-Meghna delta system. *Science of The Total Environment* 643, 1054–1064. <https://doi.org/10.1016/j.scitotenv.2018.06.147>
- Ramakrishnan, M., & Vaidyanadhan, R., 2010. *Geology of India* (vol. 1 & 2). GSI Publications, 2(1).
- Rao, V.P., Kessarkar, P.M., Thamban, M. and Patil, S.K., 2010. Paleoclimatic and diagenetic history of the late quaternary sediments in a core from the Southeastern Arabian Sea: Geochemical and magnetic signals. *Journal of oceanography* 66(1), 133-146. <https://doi.org/10.1007/s10872-010-0011-2>
- Razik, S., Dekkers, M.J. and von Dobeneck, T., 2014. How environmental magnetism can enhance the interpretational value of grain-size analysis: A time-slice study on sediment export to the NW African margin in Heinrich Stadial 1 and Mid Holocene. *Palaeogeography, Palaeoclimatology, Palaeoecology* 406, 33-48. <https://doi.org/10.1016/j.palaeo.2014.04.009>
- Razik, S., Govin, A., Chiessi, C.M., von Dobeneck, T., 2015. Depositional provinces, dispersal, and origin of terrigenous sediments along the SE South American continental margin. *Marine Geology* 363, 261–272. <https://doi.org/10.1016/j.margeo.2015.03.001>
- Roberts, A.P., 2015. Magnetic mineral diagenesis. *Earth-Science Reviews* 151, 1–47. <https://doi.org/10.1016/j.earscirev.2015.09.010>
- Sangode, S.J., Suresh, N. and Bagati, T.N., 2001. Godavari source in the Bengal fan sediments: results from magnetic susceptibility dispersal pattern. *Current Science*, 660-664. <https://www.jstor.org/stable/24104167>
- Sebastian, T., Nath, B.N., Ramaswamy, V., Mascarenhas-Pereira, M.B.L., Yazing, A.K., Apurva, P.R., Linsy, P., Kocherla, M., Miriyala, P., Rao, B.R., 2019a. Distribution and dispersal of surface sediments on the continental margins of India. *Marine and Petroleum Geology* 110, 122–137. <https://doi.org/10.1016/j.marpetgeo.2019.07.017>
- Sebastian, T., Nath, B.N., Venkateshwarlu, M., Miriyala, P., Prakash, A., Linsy, P., Kocherla, M., Kazip, A. and Sijinkumar, A.V., 2019b. Impact of the Indian Summer Monsoon variability on the source area weathering in the Indo-Burman ranges during the last 21 kyr—A sediment record from the Andaman Sea. *Palaeogeography, Palaeoclimatology, Palaeoecology* 516, 22-34. <https://doi.org/10.1016/j.palaeo.2018.11.035>
- Segall, M.P., Kuehl, S.A., 1992. Sedimentary processes on the Bengal continental shelf as revealed by clay-size mineralogy. *Continental Shelf Research* 12, 517–541. [https://doi.org/10.1016/0278-4343\(92\)90089-3](https://doi.org/10.1016/0278-4343(92)90089-3)
- Shankar, D., Vinayachandran, P.N., Unnikrishnan, A.S., 2002. The monsoon currents in the north Indian Ocean. *Progress in Oceanography* 52, 63–120. [https://doi.org/10.1016/S0079-6611\(02\)00024-1](https://doi.org/10.1016/S0079-6611(02)00024-1)
- Singh, M., Singh, I.B., Müller, G., 2007. Sediment characteristics and transportation dynamics of the Ganga River. *Geomorphology* 86, 144–175. <https://doi.org/10.1016/j.geomorph.2006.08.011>

- Singh, S.K., 2006. Spatial variability in erosion in the Brahmaputra basin: causes and impacts. *Current Science*, 1272-1276. <https://www.jstor.org/stable/24092032>
- Solangi, S.H., Nazeer, A., Abbasi, S., Zulkifil, M.M., 2019. Morphological features of continental shelf margin: Examples from the Pakistan Offshore. *Geodesy and Geodynamics* 10, 77–91. <https://doi.org/10.1016/j.geog.2018.09.004>
- Subramanian, V., Ramanathan, A.L., 1996. Nature of Sediment Load in the Ganges-Brahmaputra River Systems in India. 151–168. https://doi.org/10.1007/978-94-015-8719-8_8
- Taft, R.A. and Jones, C., 2001. Sediment sampling guide and methodologies. State of Ohio Environmental Protection Agency.
- Thompson, R., 2012. Environmental magnetism. Springer Science & Business Media.
- Thompson, R., Oldfield, F., 1986. Environmental Magnetism. Springer Netherlands, Dordrecht. <https://doi.org/10.1007/978-94-011-8036-8>
- Vaithyanathan, P., Ramanathan, A. L., & Subramanian, V., 1988. Erosion, transport and deposition of sediments by the tropical rivers of India. IN: Sediment Budgets. IAHS Publication, (174).
- Verma, R.K., Banerjee, P., 1992. Nature of continental crust along the Narmada—Son Lineament inferred from gravity and deep seismic sounding data. *Tectonophysics* 202, 375–397. [https://doi.org/10.1016/0040-1951\(92\)90121-L](https://doi.org/10.1016/0040-1951(92)90121-L)
- Wandrey, C.J. and Law, B.E., 1998. Maps showing geology, oil and gas fields and geologic provinces of South Asia: U.S. Geological Survey Open-File Report 97-470-C, 10 p. <https://doi.org/10.3133/ofr97470C>.
- Wang, K., Tada, R., Zheng, H., Irino, T., Zhou, B., Saito, K., 2020. Provenance changes in fine detrital quartz in the inner shelf sediments of the East China Sea associated with shifts in the East Asian summer monsoon front during the last 6 kyrs. *Progress in Earth and Planetary Science* 7, 5. <https://doi.org/10.1186/s40645-019-0319-5>
- Wang, Y., Wang, S. and Liu, M., 2017. Magnetic properties indicate sediment provenance and distribution patterns in the Bohai and Yellow Seas, China. *Continental Shelf Research* 140, 84-95. <https://doi.org/10.1016/j.csr.2017.04.012>
- Wasson, R.J., 2003. A sediment budget for the Ganga-Brahmaputra catchment. *Current Science* 84, 1041–1047. <https://www.jstor.org/stable/24107666>
- Whitehead, P.G., 2018. Biophysical Modelling of the Ganges, Brahmaputra, and Meghna Catchment, in: *Ecosystem Services for Well-Being in Deltas*. Springer International Publishing, Cham, 249–262. https://doi.org/10.1007/978-3-319-71093-8_13

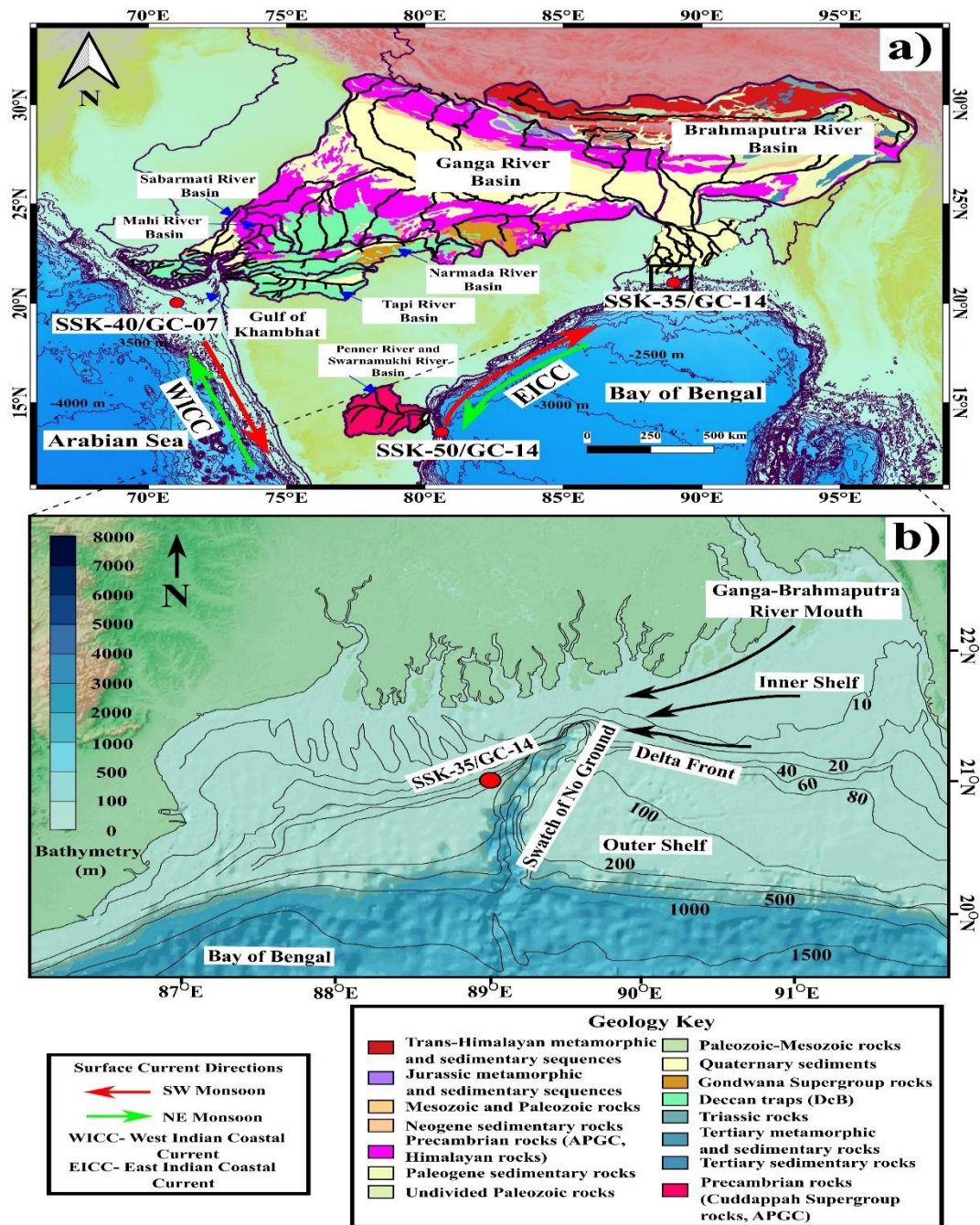


Figure. 1: a) Geological map of Narmada, Tapi, Mahi and Sabarmati (NTMS), Ganga and Brahmaputra (G-B) and Pennar and Swarnamukhi (P-S) rivers drainage area showing different lithological units. Red circles indicate the studied core locations (SSK-40/GC-07, SSK-35/GC-14 and SSK-50/GC-14). West Indian coastal current (WICC) and East Indian coastal current (EICC) are marked by green and red arrows according to their directions during the Monsoon season. Geological map is prepared using QGIS (v 3.16.8) software by extracting the shapefiles from a digitally compiled map of South Asia (USGS) (Wandrey and Law, 1998) (<https://pubs.er.usgs.gov/publication/ofr97470C>). Bathymetry contours were obtained from GEMCO 2021 Grid. APGC and DcB denote Archean Proterozoic gneissic complex and Deccan basalts respectively. b) Bathymetry map showing core SSK-35/GC-14 (off G-B) location. The positions of SoNG (Swatch of No Ground), inner shelf, delta front and outer shelf are indicated. Black arrows indicate generalized suspended sediment transport path (modified after Michels et al., 2003 and references therein).

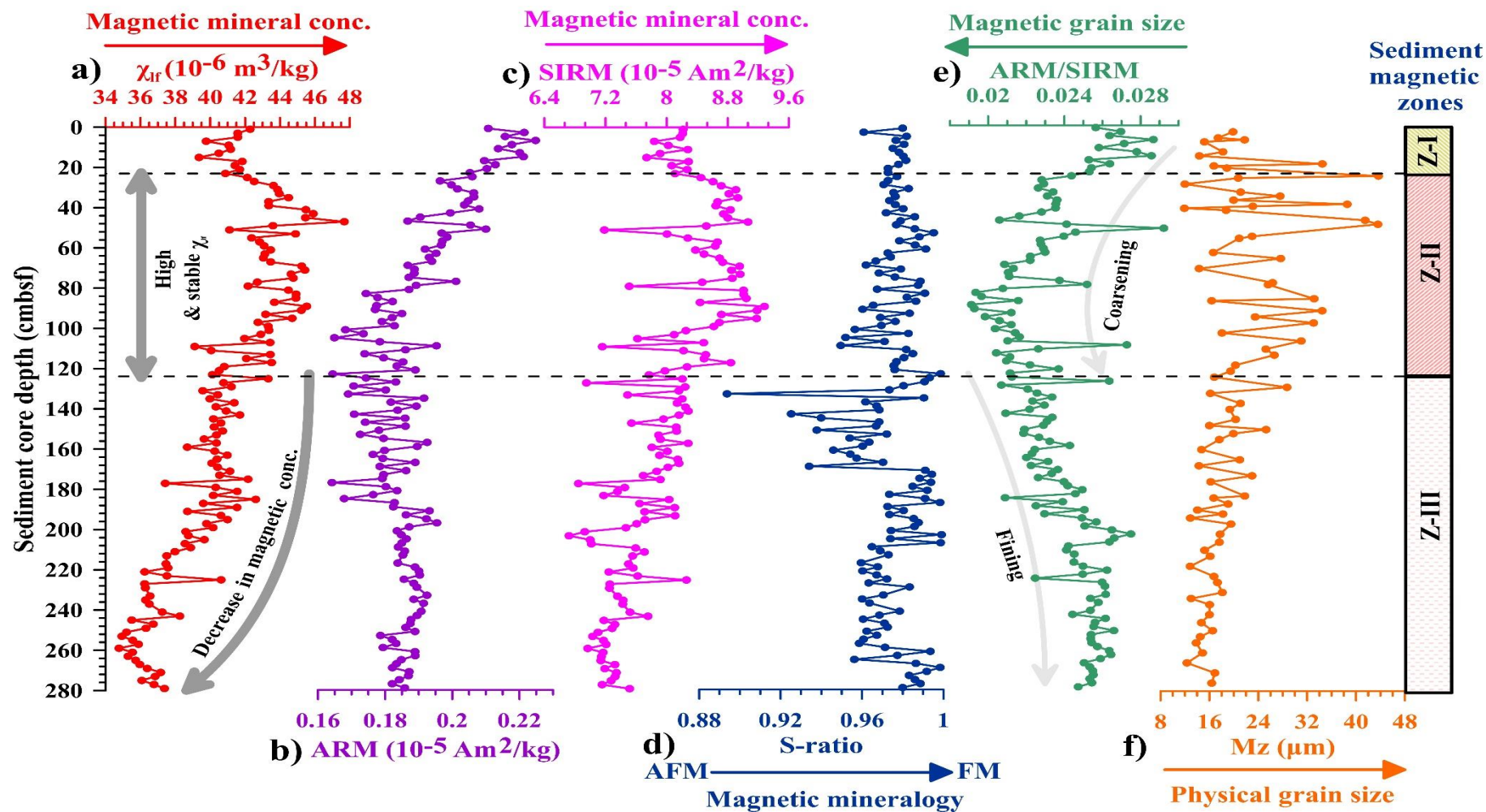


Figure 2: Plot showing downcore variations in the rock magnetic parameters and physical grain size of the sediment core from off Narmada, Tapti, Mahi and Sabarmati (NTMS) shelf (SSK-40/GC-07). Sediment magnetic zones are demarcated with dotted line. The presented rock magnetic and grain size parameters are a) magnetic susceptibility (χ_{ir}), b) anhysteretic remanent magnetization (ARM), c) saturation isothermal remanent magnetization (SIRM), d) S-ratio, e) ARM/SIRM and f) physical grain size (μm). AFM and FM denote antiferromagnetic and ferrimagnetic minerals respectively.

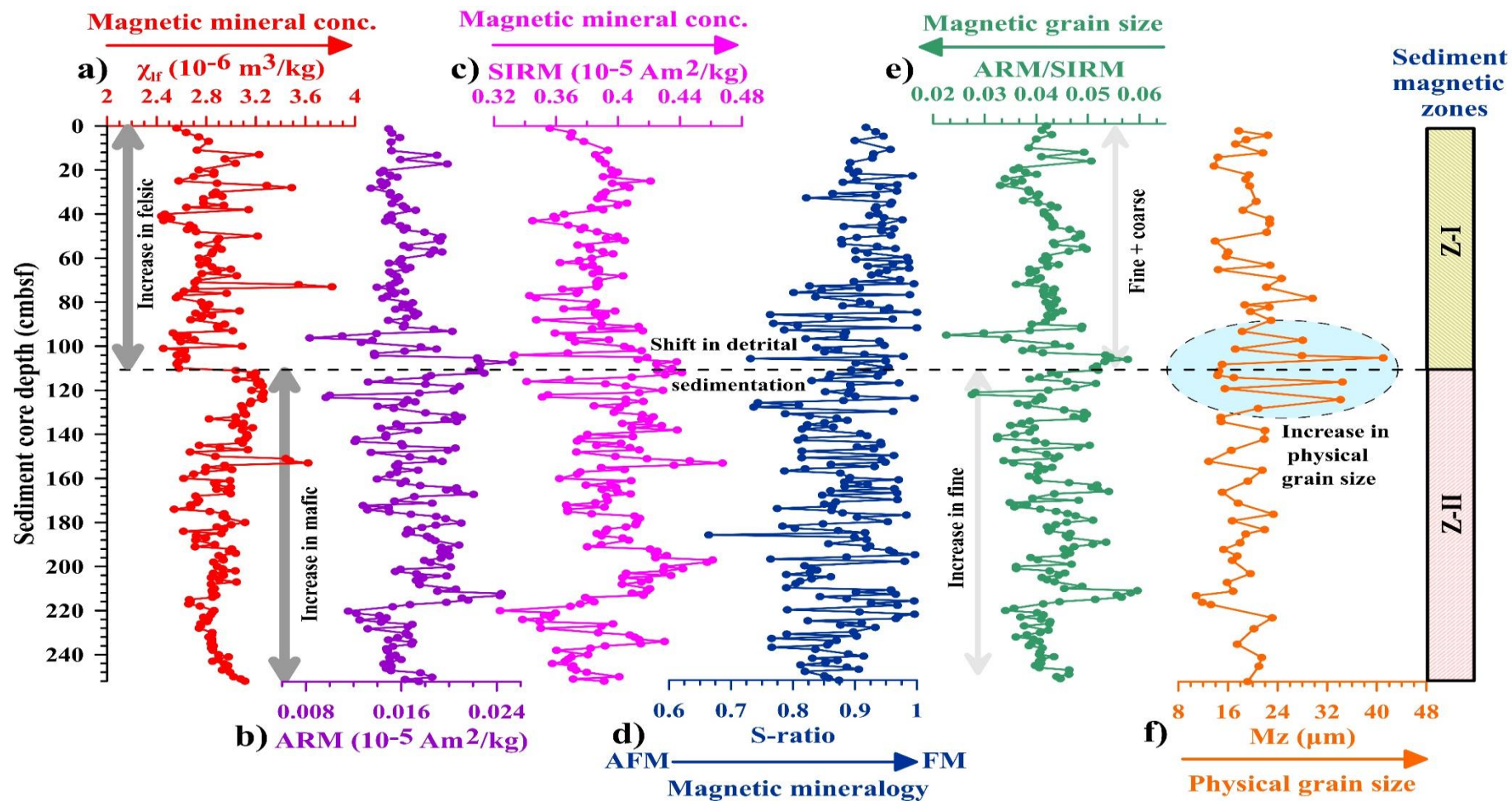


Figure 3: Plot showing downcore variations in the rock magnetic parameters and physical grain size of the sediment core from off Ganga and Brahmaputra (G-B) shelf (SSK-35/GC-14). Increase in physical grain size is highlighted using a circle filled with light blue colour. The presented rock magnetic and grain size parameters are a) magnetic susceptibility (χ_{f}), b) anhysteretic remanent magnetization (ARM), c) saturation isothermal remanent magnetization (SIRM), d) S-ratio, e) ARM/SIRM and f) physical grain size (μm). AFM and FM denote antiferromagnetic and ferrimagnetic minerals respectively.

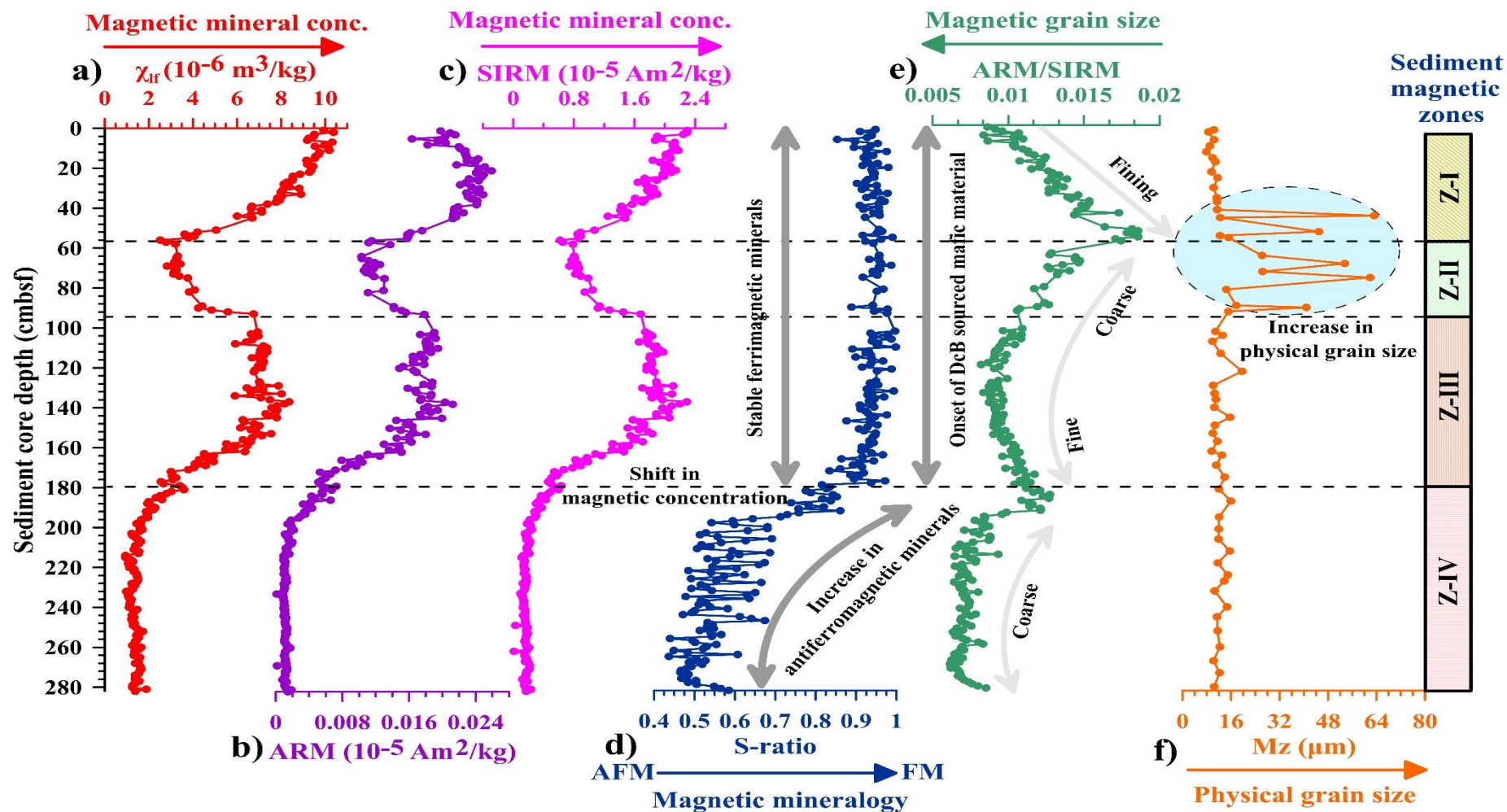


Figure. 4: Plot showing downcore variations in the rock magnetic parameters and physical grain size of the sediment core from off Pennar and Swarnamukhi (P-S) shelf (SSK-50/ GC-14). Increase in physical grain size is highlighted using a circle filled with light blue colour. Sediment magnetic zones are demarcated with dotted line. The presented rock magnetic and grain size parameters are a) magnetic susceptibility (χ_{ir}), b) anhysteretic remanent magnetization (ARM), c) saturation isothermal remanent magnetization (SIRM), d) S-ratio, e) ARM/SIRM and f) physical grain size (μm). AFM and FM denote antiferromagnetic and ferrimagnetic minerals respectively.

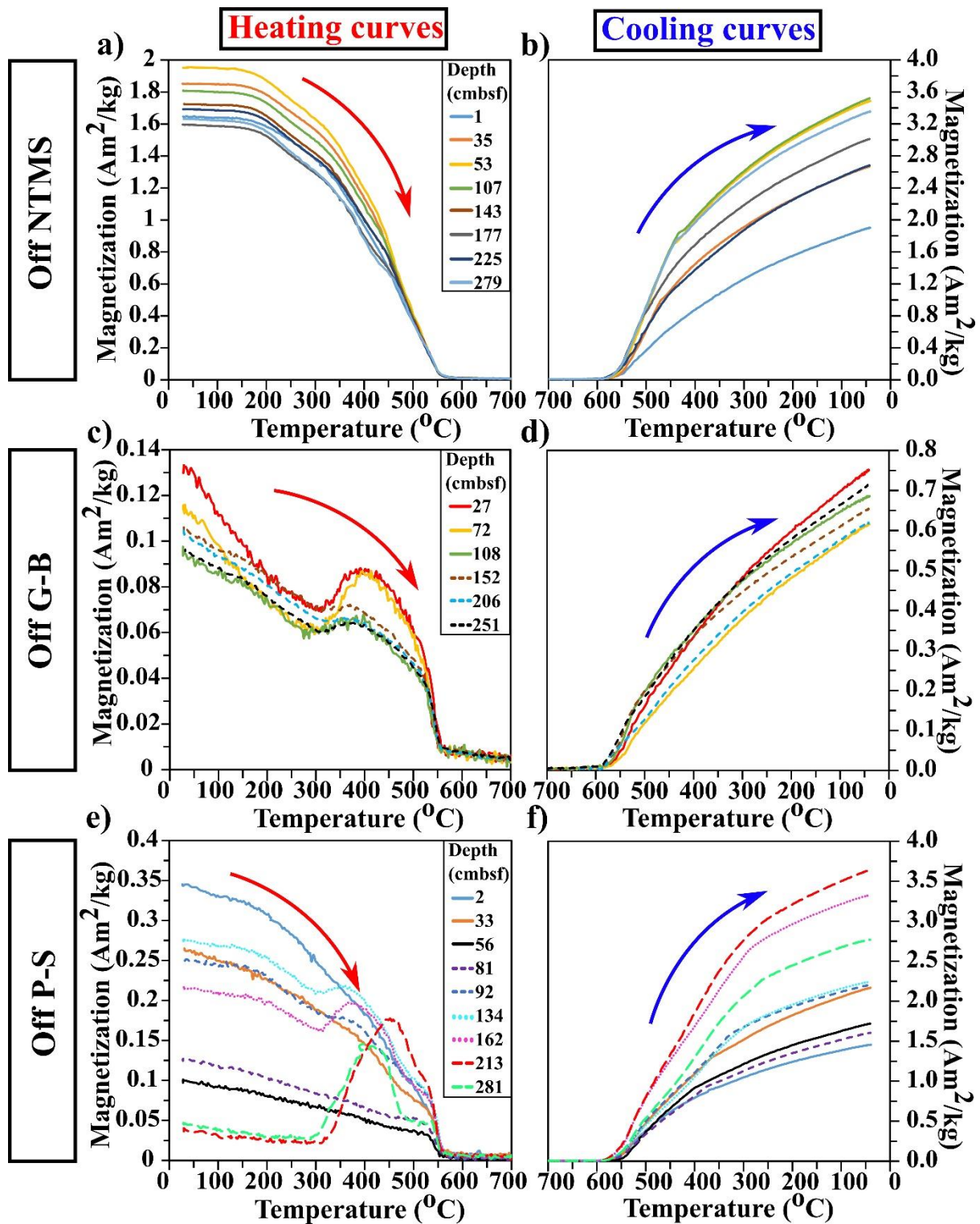


Figure. 5: Thermomagnetic curves (magnetization vs temperature) of representative samples from off Narmada, Tapti, Mahi and Sabarmati (NTMS) (SSK-40/GC-07) (a-b), off Ganga and Brahmaputra (G-B) (SSK-35/GC-14) (c-d) and off Pennar and Swarnamukhi (P-S) shelf (SSK-50/ GC-14) (e-f) core sediments. Red and blue arrows indicate heating and cooling cycles.

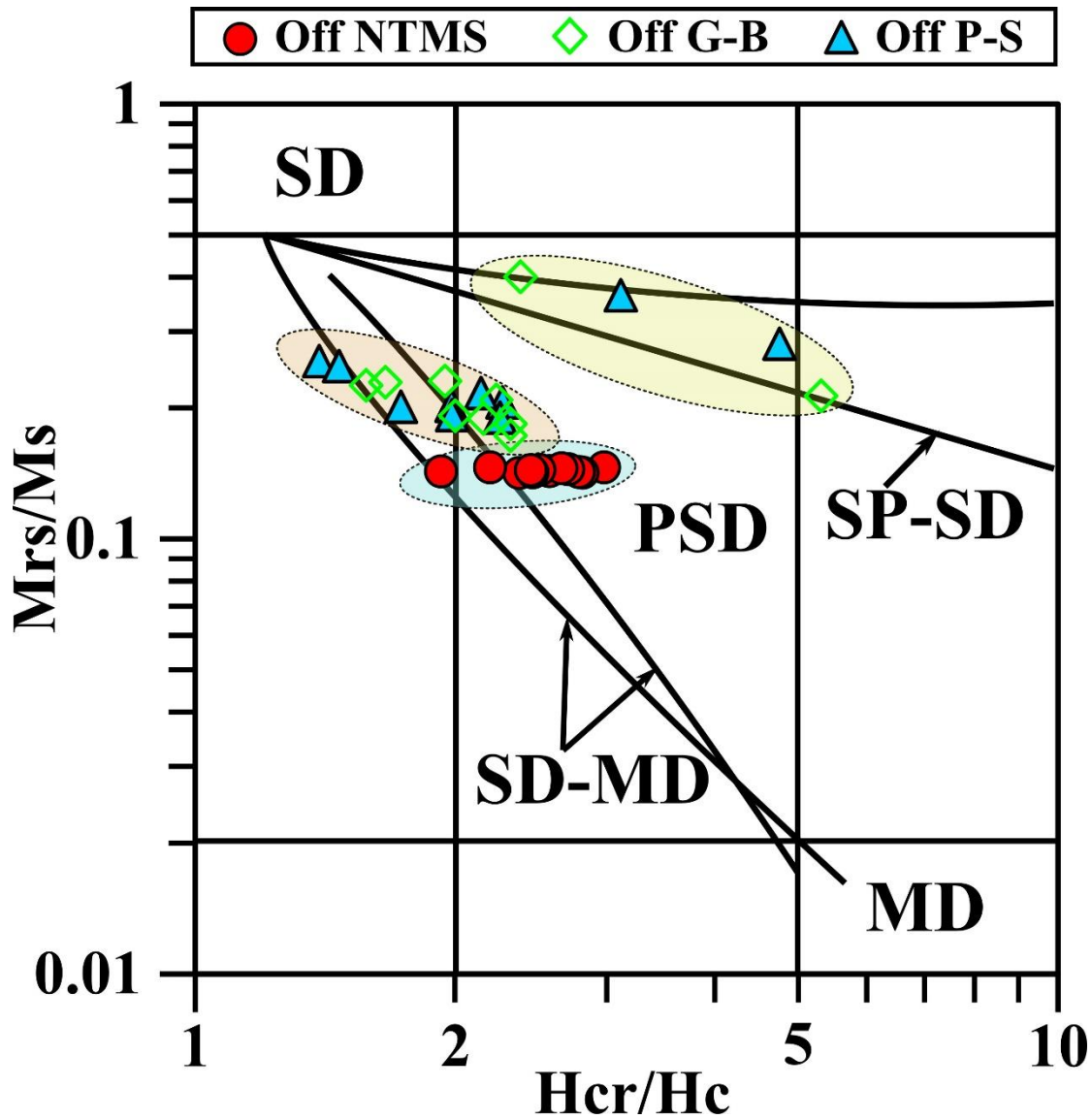


Figure. 6: Plot of H_{cr}/H_c (reduced coercivity ratio) against M_{rs}/M_s (reduced magnetization ratio) (Day et al., 1977) of representative samples from off Narmada, Tapi, Mahi and Sabarmati (NTMS) (SSK-40/GC-07) (red circles), off Ganga and Brahmaputra (G-B) (SSK-35/GC-14) (green diamonds) and off Pennar and Swarnamukhi (P-S) shelf (SSK-50/GC-14) (blue triangles) core sediments. Domain mixing lines are adopted from Dunlop (2002).

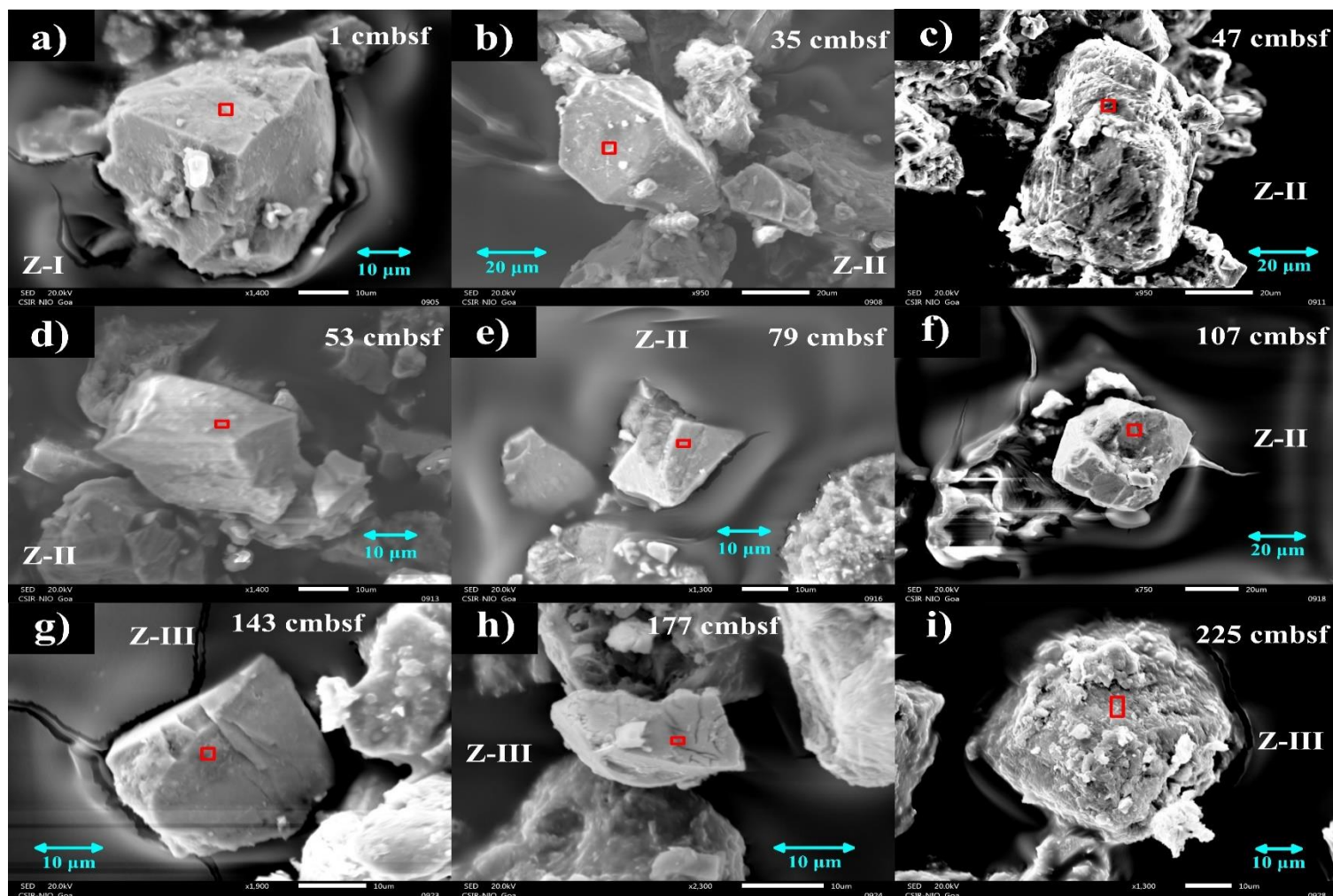


Figure. 7: Scanning electron microscopic (SEM) images (a-i) of selected samples at different depth intervals (sediment magnetic zones: Z-I, Z-II & Z-III) from the sediment core off Narmada, Tapti, Mahi and Sabarmati (NTMS) (SSK-40/GC-07) shelf. Energy dispersive spectra's (EDS) are presented in a supplementary figure (Fig. S10). The position of the spectra is shown by red coloured rectangle.

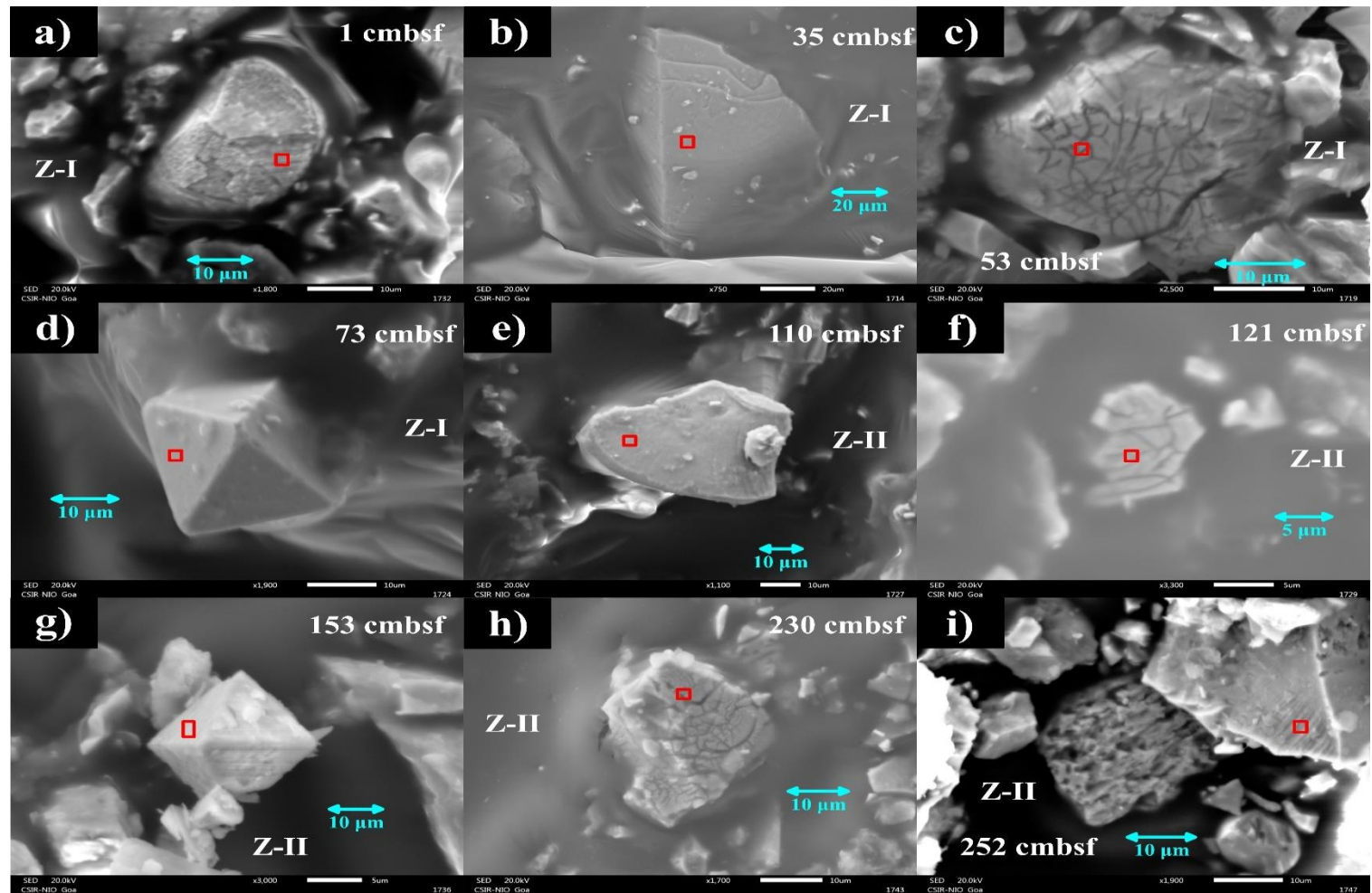


Figure. 8: Scanning electron microscopic (SEM) images (a-i) of selected samples at different depth intervals (sediment magnetic zones: Z-I & Z-II) from the sediment core off Ganga and Brahmaputra (G-B) (SSK-35/GC-14) shelf. Energy dispersive spectra's (EDS) are presented in a supplementary figure (Fig. S11). The position of the spectra is shown by red coloured rectangle.

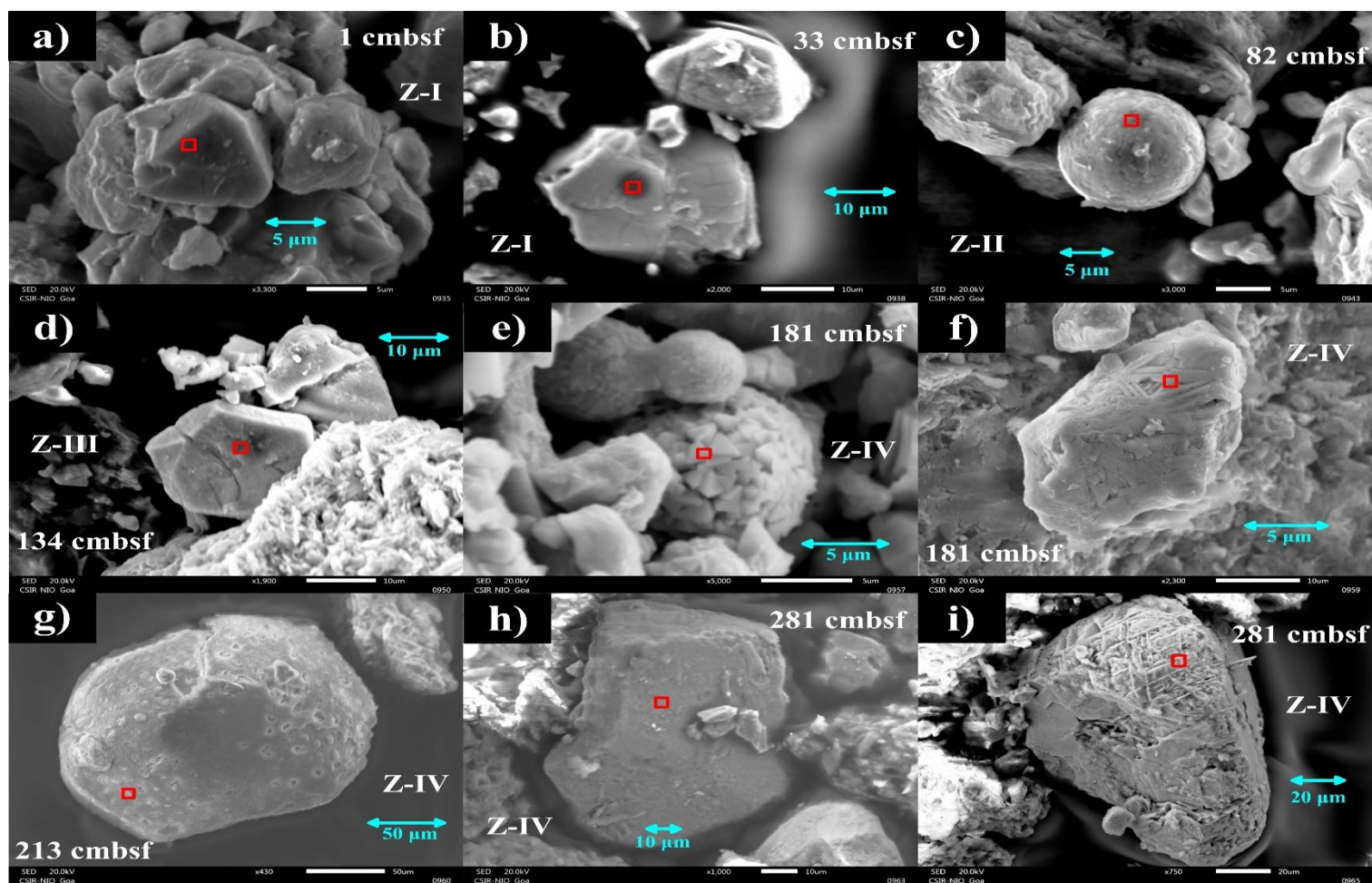


Figure. 9: Scanning electron microscopic (SEM) images (a-i) of selected samples at different depth intervals (sediment magnetic zones: Z-I, Z-II, Z-III & Z-IV) from the sediment core off Pennar and Swarnamukhi (P-S) (SSK-50/GC-14) shelf. Energy dispersive spectra's (EDS) are presented in a supplementary figure (Fig. S12). The position of the spectra is shown by red coloured rectangle.

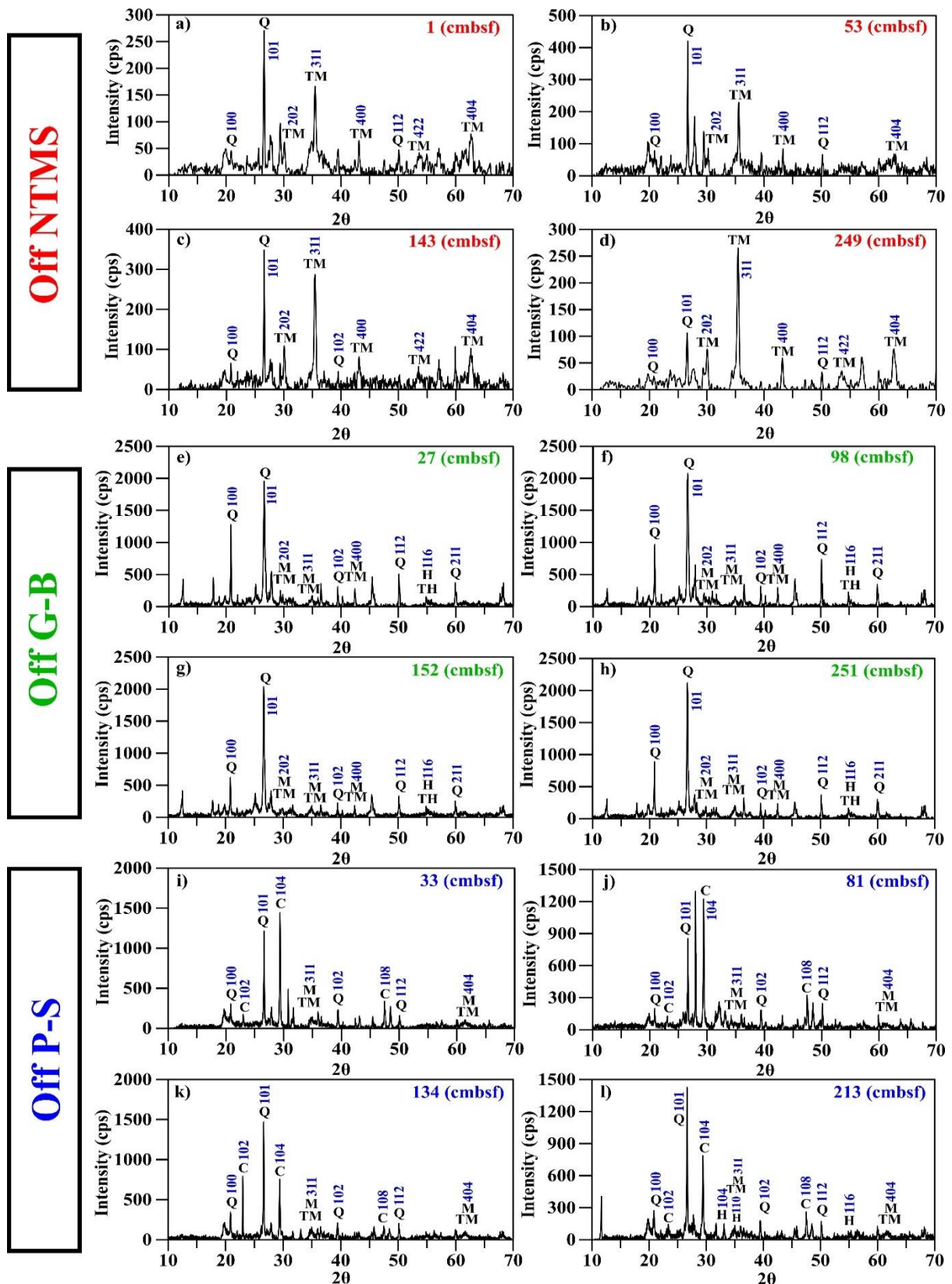


Figure 10: X-ray diffractograms (XRD) of magnetic mineral extracts (off Narmada, Tapi, Mahi and Sabarmati (NTMS) (SSK-40/GC-07)) and bulk sediments (off Ganga and Brahmaputra (G-B) (SSK-35/GC-14), off Pennar and Swarnamukhi (P-S) shelf (SSK-50/ GC-14)) at different depth intervals. The peaks of Quartz (Q), magnetite (M), titanomagnetite (TM), hematite (H), titanohematite (TH) and calcite (C) are specified.

River	River length (km)	Drainage area ($\times 10^5$ km ²)	Sediment load (Mt)	References
Narmada	1312	0.99	69.7	Panda (2011)
Tapi	724	0.65	24.7	
Mahi	583	0.35	9.7	
Sabarmati	371	0.22	-	
Penner	597	0.55	7	Vaithyanathan et al. (1988)
Swarnamukhi	192	0.03	-	Patel et al. (2020)
Ganga	2525	10.87	150-590	Rahman (2018)
Brahmaputra	2880	5.43	135-615	Rahman (2018)

Table 1: Details of the river length, drainage area and sediment load of rivers NTMS, G-B and P-S.

Sr. No.	Core ID	Water Depth (m)	Core location	Site		Core length (mbsf)	Magnetic susceptibility (χ_{lf}) (10^{-6} m ³ /kg)				Magnetite content (wt %)			
				Latitude (°N)	Longitude (°E)		Max.	Min.	Avg.	S.D.	Max.	Min.	Avg.	S.D.
1	SSK-40/GC-07	68	Off NTMS	20° 1' 48"	71° 2' 24"	2.79	47.68	34.78	40.65	2.92	7.22	5.27	6.16	0.04
2	SSK-35/GC-14	53	Off G-B	21° 2' 24"	88° 59' 24"	2.53	3.81	2.44	2.89	0.22	0.58	0.37	0.44	0.03
3	SSK-50/GC-14	411	Off P-S	13° 31' 12"	80° 36' 0"	2.83	10.38	0.95	4.47	2.96	1.57	0.14	0.68	0.45

Table 2: Details of the core location, core length, water depth, magnetic susceptibility and magnetite content in the shelf sediments off NTMS, off G-B and off P-S.